POLITECNICO DI TORINO

DENERG – Energy Department

Master of Science in Energy and Nuclear Engineering

Master Thesis

"Development of a Dedicated Graphical User Interface and Experimental Tests to Extract the Parameters of Equivalent Circuit for a Commercial Photovoltaic Module"

Supervisors: **Candidate:**

Prof. Filippo Spertino   Hafsa Siddiqi

Prof. José Vicente Muñoz Díez

Ing. Gabriele Malgaroli

October,2021

Academic Year 2020/2021

Acknowledgement

I thank Prof. Filippo Spertino, Eng. Gabriele Malgaroli and Prof. Vicente Munoz for assisting me in this work with great patience and availability. In particular, with a warm heart, I thank Gabriele for putting up with his infinite efforts and Vicente for welcoming me to Jaén, not making me feel homesick. I thank my friends who have been close to me and with whom I have distracted myself and relaxed during my long university career. I thank Muhammad Aoun Ejaz Qureshi for being a great companion during my thesis. Moreover, heartfelt thanks go to my parents, who have always supported me emotionally and financially during this university period. Indeed, without your help, I would not have been able to get this far.

Hafsa Siddiqi

Table of Contents

Academic year 2020/2021

List of Figures

v

List of Tables

Glossary of Acronyms

Acronyms	Meanings
CIEMAT	"Centro de Investigaciones Energéticas, Medioambientales y Tecnológicas" in Madrid
AM	Air Mass
ADC	Analog-to-Digital Converter
FF	Fill Factor
GUI	Graphical User Interface
IDEA	Grupo de Investigación y Desarrollo en Energía Solar y Automática
LM	Levenberg-Marquardt algorithm
MPP	Maximum Power Point
MPPT	Maximum Power Point Tracker
NOCT	Nominal Operating Cell Temperature $(G_{NOCT} = 800\ Wm^{-2}, T_{c,NOCT} = 20\ °C, WS_{NOCT} = 1\ ms^{-1})$
NRMSE	Normalized Root Mean Square Error
OC	Open Circuit
PV	PhotoVoltaic
SC	Short Circuit
RTD	Resistance Temperature Detector
5P	Single diode 5 parameters model
STC	Standard Test Condition $(G_{STC} = 1000\ Wm^{-2}, T_{c,STC} = 25\ °C, AM\ 1,5)$
TRC	Temperature Coefficient of Resistance
Pt100	Temperature sensor ("Pt" platinum, "100" resistance in Ω at 0 °C)
UJA	Universidad de Jaén
I-V	Voltage and current characteristics of photovoltaic generator
P-V	Voltage and power characteristics of photovoltaic generator
PoliTO	Politecnico Di Torino

Table of Constants

Symbols	Significance	Value	Units
Ta,NOCT	Air temperature in NOCT	25	°C
k_b	Boltzmann constant	$1{,}38.10^{-23}$	$J \cdot K^{-1}$
q_e	Electron charge	$1{,}602.10^{-19}$	C
G_{NOCT}	Module (or cell) irradiance in NOCT	800	Wm^{-2}
G_{STC}	Module (or cell) irradiance in STC	1000	Wm^{-2}
$T_{C,STC}$	Module (or cell) temperature in STC	25	°C
h	Plank constant	$6{,}626 .10^{-34}$	$J \cdot s$
α_{Pt100}	Pt100 temperature coefficient	0.00385	$\Omega \cdot \Omega^{-1} \cdot K^{-1}$
c	Speed of light in vacuum	$2{,}998 .10^{8}$	$m \cdot s^{-1}$

Glossary of Symbols

Symbols	Meaning	Unit
χ	A-dimensional empirical coefficient of the diode saturation current	-
T_a	Ambient Air Temperature	°C
APE	Average Photon Energy	eV
C	Capacitor Capacitance	F
t_c	Capacitor charging time	s
I	Current	A
I_{model}	Current (estimated from model)	A
I_{exp}	Current (experiment value)	A
I_j	Current in the diode (5P model)	A
I_{sh}	Current in the parallel resistance (5P model)	A
I_{MPP}	Current point in MPP	A
$I_{0,\,STC}$	Diode saturation current at STC	A
G	Irradiance	$W \cdot m^{-2}$
E_{model}	Energy (estimated from model)	J
E_{exp}	Energy (experimental value)	J
E_g	Energy gap	J
$E_{g,STC}$	Energy gap at STC	J
E_{ph}	Energy of the photon	J
X_{cor}	Estimation from correlation parameter X value	-
X_{exp}	Experimental parameter X value	-
ν	Frequency	Hz
b	Ideality factor correlation effect in irradiance	$W^{-1} \cdot m^2$
c	Ideality factor correlation effect in temperature	C^{-1}
a	Ideality factor correlation intercept	-
n	Ideality factor of the diode (5P model)	-

$P_{Osterwald}$ Power at MPP by the Osterwald method   W $\cdot$m^{-2}

Introduction

The operation of photovoltaic generators can be defined using an equivalent circuit with a varying number of parameters, which are, usually, presumed to be constant. Nevertheless, the knowledge of their dependence with respect to irradiance and cell temperature allows to foresee the generated power of photovoltaic arrays in any weather condition. Furthermore, the knowledge of the parameters in any condition permits to draw the current-voltage (I-V) characteristic curve of the photovoltaic generators. This knowledge might be used in future works to estimate the state of health of photovoltaic arrays by studying the shape of the I-V curve and the values of circuit parameters can be estimated in any environmental condition.

This thesis emphasis on the experimental validation of an innovative technique to predict the parameters of the equivalent circuit in any weather condition. This work is a part of a joint activity between Politecnico di Torino and the Universidad de Jaén (Spain): my main activity of this thesis has been developed in Universidad de Jaén.

For this thesis a Graphical User interface (GUI) is developed in MATLAB to allow the wide analysis of a huge dataset of experimental data. Specifically, the tool permits to execute four operations: the preprocessing of the dataset; the extraction of the circuit parameters; the identification of equations, aiming at describing the dependence of each parameter with respect to irradiance and cell temperature, and the comparison between experimental energy can be predicted by various methods. Experimental data might be influenced by measurements errors, or by the photovoltaic generators that might work in mismatch conditions as a result of shadowing or other issues. Nevertheless, the current analysis involves experimental measurements of photovoltaic generators accurately operating. Therefore, the preprocessing step eliminates the problematic measurements integrating filters. Initially, the experimental data with measurement errors are filtered by assessing the irradiance and the temperature detected by the sensors: for the high deviations among the measured quantities, the empirical data are excluded. Later, the

measurements obtained on cloudy/partly cloudy days with unexpected irradiance variations or I-V curves with mismatch are removed.

The parameters extraction step is the important tool: in this step, the parameters are mathematically determined starting from the filtered measurements. The GUI allows to recognize the circuit parameters with the help of two circuit models and algorithms. The third step of the analysis is the identification of the dependence of circuit parameters with respect to cell temperature and irradiance. Specifically, the most common equations in literature are used and a nonlinear optimization of specific coefficients is performed. At last, the generated energy during the experimental campaign is compared to the associated value by several methods. The GUI permits to estimate the expected energy using theoretical models and the optimized equations: starting from the of the parameters, the I-V curve are drawn at each time step and the resultant maximum power is identified.

Finally, the GUI is used for a multi crystalline silicon module of Kyocera with rated power of 135W. The experimental campaign lasted for four months. Additionally, the single diode model is used which is the conventional circuit model in literature. About the numerical algorithms, the Levenberg Marquardt algorithms is implemented. Lastly, the results of energy estimation are evaluated between experimental data, the optimized equations and the Osterwald model (the most common theoretical model in literature to estimate photovoltaic power).

Chapter 1: Photovoltaic Technology

All energy on Earth has been created by solar power. It is the fundamental energy that sustains every process on Earth: from the photosynthesis of plants to the production of fossil fuels and wind and hydroelectric energy. Therefore, it can be said that solar energy is the most abundant source of energy available. In other words, if it could be entirely converted into usable energy, the sunlight that reaches the Earth in a day could be enough to address the world's needs for a whole year.

1.1 Solar Energy

Solar energy is a renewable source that is generated from sunlight. Sunlight is a form of electromagnetic radiation that precisely consists of a range of energy bands called the solar spectrum. In this regard, the solar spectrum is divided into different wavelengths that are distinguished by different energies. The most dominant component of the spectrum is ultraviolet radiation (UV), visible radiation and infrared radiation (IR). Most of the UV radiation is filtered out by the atmosphere and never reaches the surface, as the energy that reaches the Earth's surface is mainly made of visible radiation (400 to 700 nm). [1] [2]

The electromagnetic spectrum describes the range of frequencies with a particular wavelength. Nevertheless, for the photovoltaic technologies, the behaviour of light can be described according to the Planck definition: The particles of energy with a quantum of radiant that travel at the speed of light. These particles are called photons. Each photon is identified by either a wavelength or energy, which are inversely proportional with each other. The following equation gives the photon energy:

$$E = \frac{h.c}{\lambda}$$
<div align="right">Equation 1</div>

Whereas:

- Planck's constant $(h) = 6.626 \cdot 10^{-34} (m^2 Kg/s)$

- Speed of light $(c) = 3 \cdot 10^{-8} \ (ms)$

- $\lambda \ (\mu m)$, is the wavelength

While dealing with particles electron volts is consider as the unit. So, the equation becomes:

$$E_{ph} = \frac{1.24 eV}{\lambda}$$
<div align="right">Equation 2</div>

This Equation helps to understand the interaction of sunlight with the p-n junctions within the solar cells. The second parameter can also be estimated to number of electrons which are generated, and therefore the current produced, in a solar cell. The photon flux can be defined as:

$$\emptyset_{Ph} = \frac{n. \ of \ photons}{m^2 \ sec}$$
<div align="right">Equation 3</div>

The estimated power density for photons at a wavelength is the combination of the photon flux and the photon energy used.

One of the most critical parameters that portray the behaviour of the PV modules is solar irradiance, which is defined as the power per unit area received from the Sun in the form of electromagnetic radiation. There are several types of irradiances:

1. Total Solar Irradiance (TSI): is the mean level of solar radiation that falls on a unit area normal to the line from the Sun per unit time outside the Earth's atmosphere.

<div align="center">4</div>

2.Direct Normal Irradiance (DNI): is the amount of solar radiation received per unit area by a surface normal to the rays that come in a straight line from the sun's direction at its current position in the sky.

3. Diffuse Horizontal Irradiance (DHI): the amount of radiation received per unit area by a surface that does not arrive on a direct path from the sun but has scattered by molecules and particles in the atmosphere that comes equally from all directions.

4. Global Horizontal Irradiance (GHI): is shortwave radiation from above by a horizontal surface.

Taking into consideration the solar irradiance, we can identify the clear sky condition. condition signifies sky without clouds and daily irradiance curves appear to be the following:
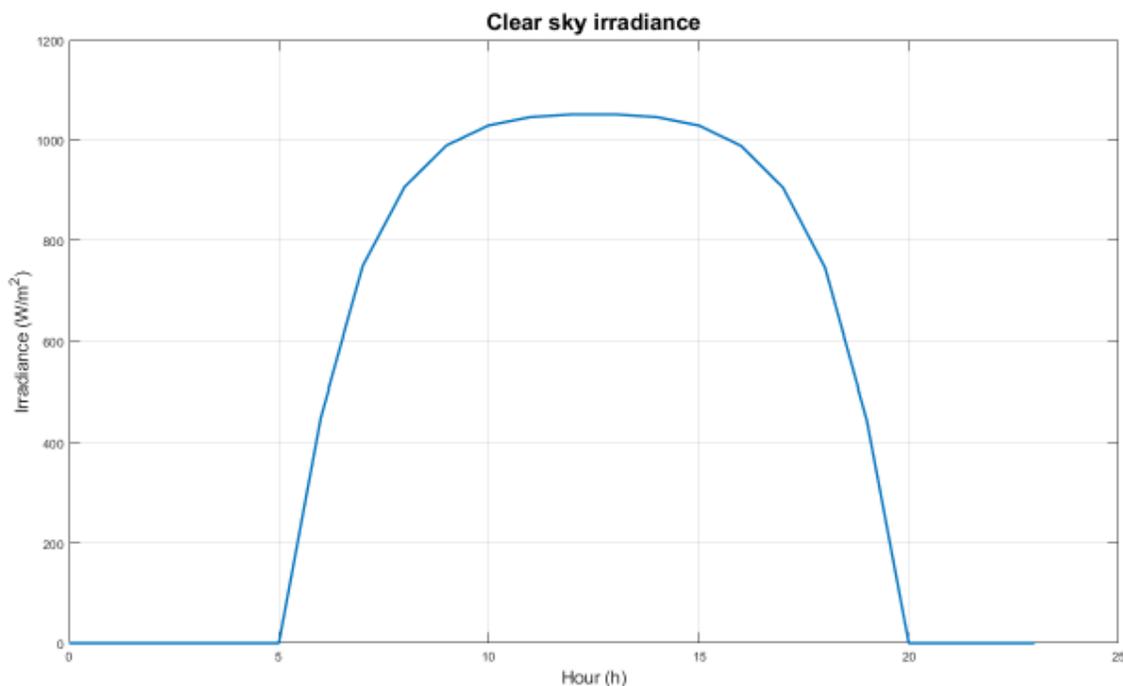
Figure 1 Daily curve of clear sky irradiance

Whereas the second most important parameter is air mass. The air mass a measure of the optical length of the atmosphere. At sea level, when the sun is completely overhead (zenith angle = 0), the air mass is equal to 1. As the zenith angle becomes larger, the path of direct sunlight through the atmosphere grows longer and air mass increases. On the other hand, land elevation

5

increases, the thickness of the atmosphere lessens, and the air mass is reduced. The relative air mass is simply a trigonometric function of the zenith angle:

$$AM = \frac{1}{COS(\theta)}$$

Equation 4

1.2 Electronic Band Structure

The band structure is responsible for the explanation of the electrical properties of a material. The energetic levels in atoms and molecules can be discrete or split into a near-continuum of levels called a band. The energy bands can represent as empty, filled, mixed or forbidden bands. The electrons occupy the energy levels. They start with the lowest energy value level. The electrons that contribute to the electrical conduction occupy the higher energy bands. The valence band relates to the highest energy band that covers electrons. The valence band can be fully or partially occupied. The permitted empty states in the valence band add a role to the electric current. The conduction band is the lowest energetic band with unoccupied states.

In materials, the conducting bands of empty, filled or permitted states can interfere with prohibited bands, also called band gaps. The width of the bandgap determines the type of material:

- *Conductors,* since the energy gap is shallow, most electrons already have the necessary energy to reach the conduction band and conduct.

- *In insulating materials*, the energy gap is very high; therefore, electrons need considerable energy to reach the conduction band, which rarely happens.

- *Semiconductors*, the situation is intermediate between an insulating material and a conductor.

6
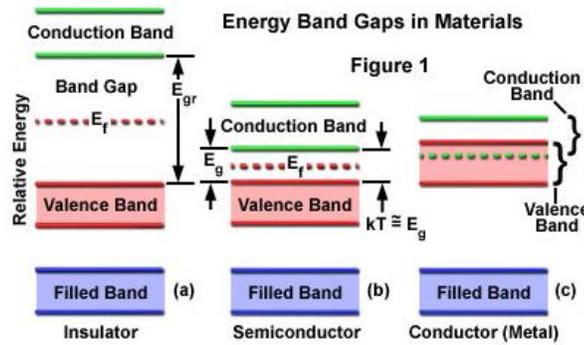
Figure 2 Band structure model of different materials: (a) insulators - (b) semiconductors - (c) conductors

1.3 Current -Voltage (I-V) Characteristic Curve of a Solar Cell

Solar Cell I-V Characteristic Curves exhibit the current and voltage (I-V) characteristics of a particular photovoltaic (PV) cell, module or array, giving a comprehensive description of its solar energy conversion ability and efficiency. Realizing the electrical I-V characteristics (more importantly, Pmax) of a solar cell or panel is critical in defining the device's output performance and solar efficiency.

The main electrical characteristics of a PV cell or module are summary in the relationship between the current and voltage produced on a typical solar cell I-V characteristics curve. The strength of the solar radiation that hits the cell controls the current (I), while the rises in the temperature of the solar cell reduce its voltage (V).

Solar Cell I-V Characteristics Curves are a graphical representation of the function of a solar cell or module reviewing the relationship between the current and voltage at the given conditions

7

of irradiance and temperature. I-V curves provide the information required to construct a solar system to operate as close to its optimal peak power point (MPP) as possible.
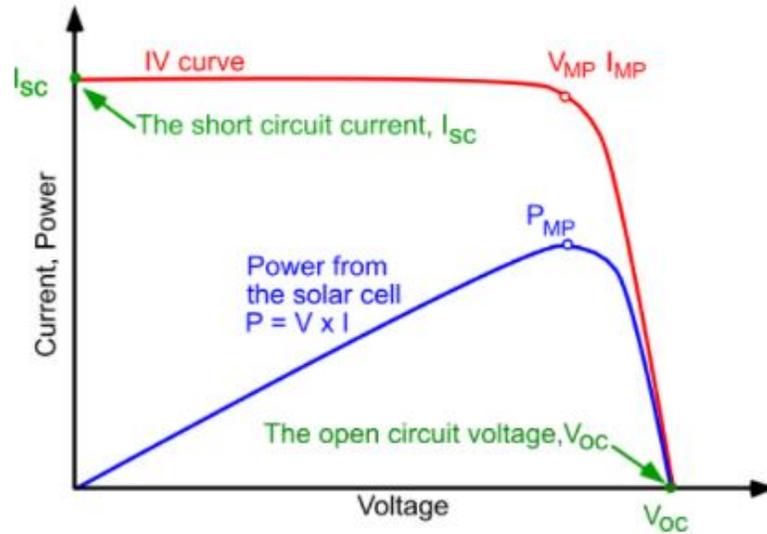
Figure 3 Current voltage (IV) cure of a solar cell. (Source PV Education)

Some main characteristics to be defined:

- V_{OC} is the open circuit voltage (V)
- I_{SC} is the short circuit current, the maximum current at zero voltage (A)
- P_{MPP} is the point of maximum power produced by the cell (W). This power is the ideal operating point. The current and voltage values that correspond to P_{MPP} are called maximum power current I_{MPP} and maximum power voltage V_{MPP}, respectively.

There are four basic properties of the I-V curve connected with V_{OC} and I_{SC}. The first is that tension increases logarithmically with irradiation. V_{OC} decreases as the temperature increase. These dependencies are translated into the following simplified formula. In fact, dependence on irradiance does not appear.

$$V_{OC}(T) = V_{OC,STC} * \left(1 + \beta_{VOC} * (T_C - T_{C,STC})\right) \qquad \text{Equation 5}$$

Where:

- $V_{OC,\,STC}$ is the open circuit voltage in STC conditions (see 2.2) (V)

- β_{VOC} is the OC voltage temperature coefficient (°C^{-1})

- T_C is the cell temperature (°C)

- $T_{C,\,STC}$ is the cell temperature in STC (°C)
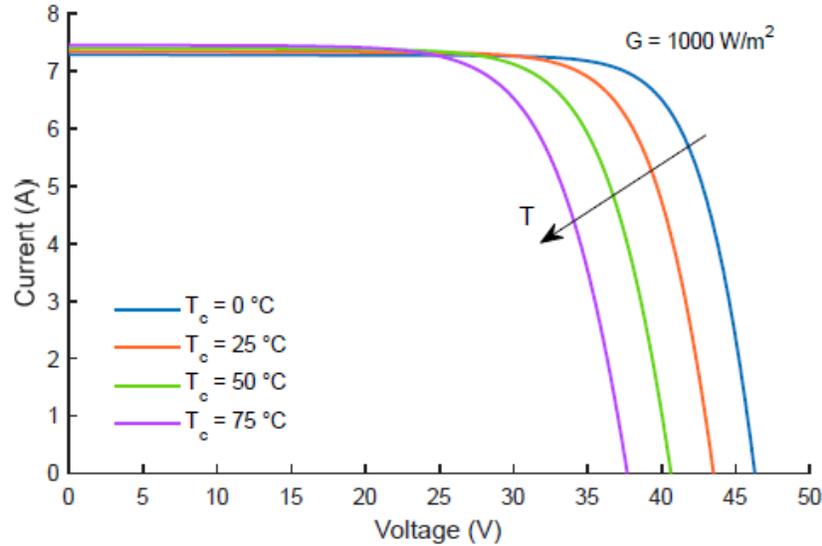
Figure 4 Dependence of the I-V curve on temperature

The third is that current is directly proportional to radiation. I_{SC} increases slightly as the temperature rises.

$$I_{SC}(G, T_C) = I_{SC,STC} * \frac{G}{G_{STC}} * \left(1 + \alpha_{Isc} * \left(T_C - T_{C,STC}\right)\right)$$
Equation 6

Where:

- $I_{SC,\,STC}$ is the short circuit current in STC conditions (see 2.2)

- G is the incident irradiance (W · m^{-2})

- G_{STC} is the incident irradiance in STC (see 2.2) (W · m^{-2})

- α_{Isc} is the SC current temperature coefficient (°C^{-1})

9
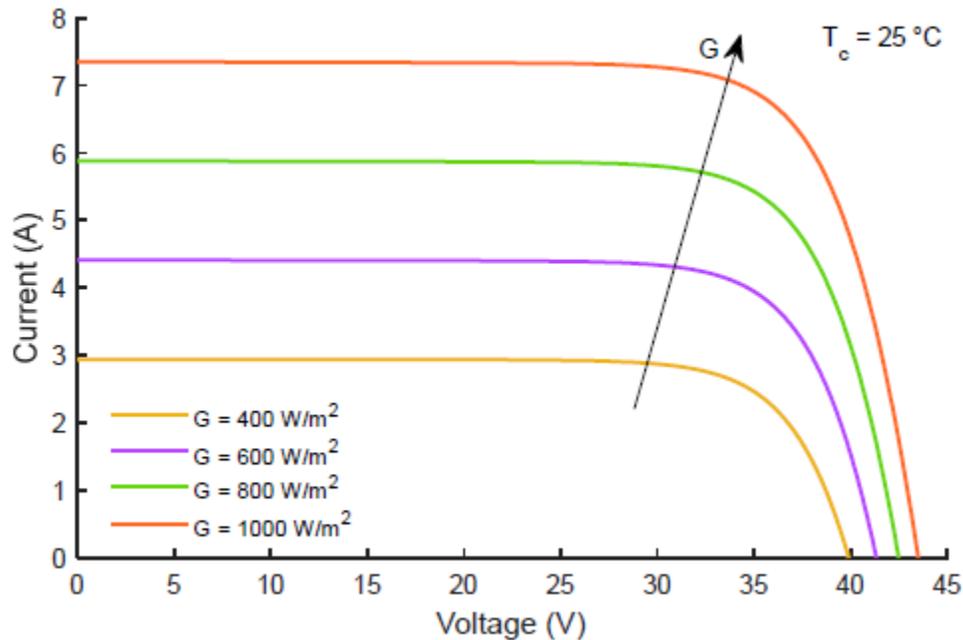
Figure 5 Dependence of the I-V curve on irradiance

1.4 Series and Parallel Connections of Photovoltaic Cells

Photovoltaic panels can be wired or connected in either series or parallel combinations, or both to increase the voltage or current capacity of the solar array. When the cells are connected in series, they are crossed by the same current and the resulting voltage is the sum of the voltages of each cell. When cells are connected in parallel, they are characterized by the same voltage and the resulting current is the sum of the currents of each. Figure 6 shows how to graphically obtain the curve of a module or a PV generator with the connections in series and parallel.
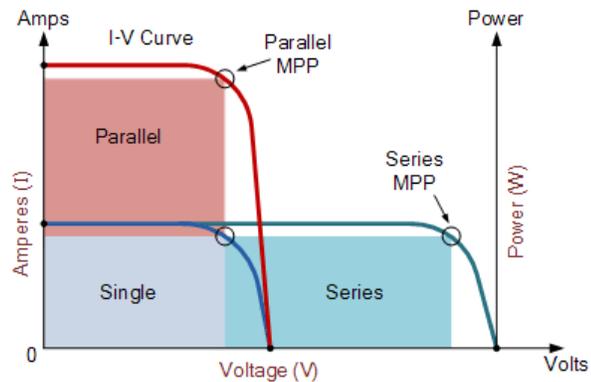
Figure 6 Series and parallel of equal I-V curves. (Source PV Education)

During the normal operation, the characteristics of the PV module show some variations due essentially to two reasons: the natural variation of parameters due to defects in manufacturing and the various working conditions that occur. These variations provoke a reduction of the performances of the PV module and are referred to the so-called mismatching. The mismatch can provoke several problems according to the connection of the cells.

1.4.1 Series Connection

If Ns identical cells are series connected and one of them has a characteristic which differ from the others, for example because of partial shading, the resulting characteristics is given by the sum, for a given current, of the voltage of the not shaded $Ns - 1$ cells and of the voltage of the shaded cell.

11
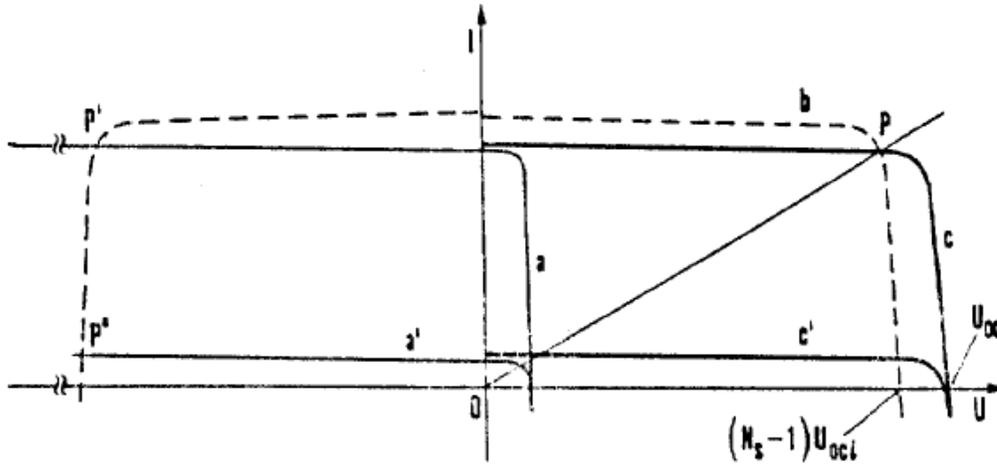
Figure 7 I-U characteristic of series connected cells in case of mismatch.

• Curve a: different from the others because of manufacturing defects.

• Curve a': different from the others because of shading.

 • Curve b: resulting from the sum of the characteristics of $Ns - 1$ normally operating cells.

 • Curve c: resulting characteristic (for the curve a), for a given current, of the voltage of the $Ns - 1$ equal cells plus the voltage of the cell with a manufacturing defect.

Curve c: resulting characteristic (for the curve a'), for a given current, of the voltage of the $Ns - 1$ equal cells plus the voltage of the shaded cell.

The maximum generated power is anyway always lower than the sum of the maximum powers of the series connected cells. The resulting curve has an open circuit voltage Uoc equal to the sum of the $U_{oc,\,i}$ of the single cells and a short circuit current Isc equal to the one of the cells which generates the lowest current.

If the cell is completely shaded, it stops generating current and starts opposing to the current flux generated by the other cells and with its own resistance generates a voltage opposed to the ones of the other cells. The shaded cells becomes then a load and it will dissipate heat creating a hot spot (point P' of Figure 8). If the voltage $(Ns-1)\,U$ exceeds the maximum break down voltage U_b, the immediate destruction of the cell occurs.

12

A diode D_P parallel connected to the shaded cells avoids that this cell operates as a load with an inverse voltage.
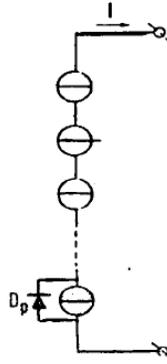
Figure 8 Protection Diode parallel connected to the solar cell.

The diode D_P has the task not to limit the short circuit current of the string to the value of the short circuit current of the cell with the worst characteristic (a') but instead the diode should make it equal to the one of the remaining series connected cells with the best characteristics.

1.4.2 Parallel Connection

As for the series connection, if N_P are parallel connected and one cell show a different characteristic from the other cells (for example because of shading), the resulting characteristics is given by the sum, for a given voltage, of the currents of the $N_P - 1$ not shaded cells and of the one of the shaded cells. The resulting characteristic has a short circuit current I_{SC} equal to the sum of $I_{SC,i\,of}$ the single cells and an open circuit voltage U_{OC} very close to the one of the shaded cells.- If one cell is shaded, the parallel of the cells behaves towards the load as the parallel of $N_P - 1$ lighted cells. The worst condition for the shaded cell is with a null external load because in this condition the shaded cell is obliged to absorb the current of the $N_P - 1$ lighted cells.

A diode D_S series connected to the cell in parallel could avoid that the shaded cells work as a load with an inverse current.
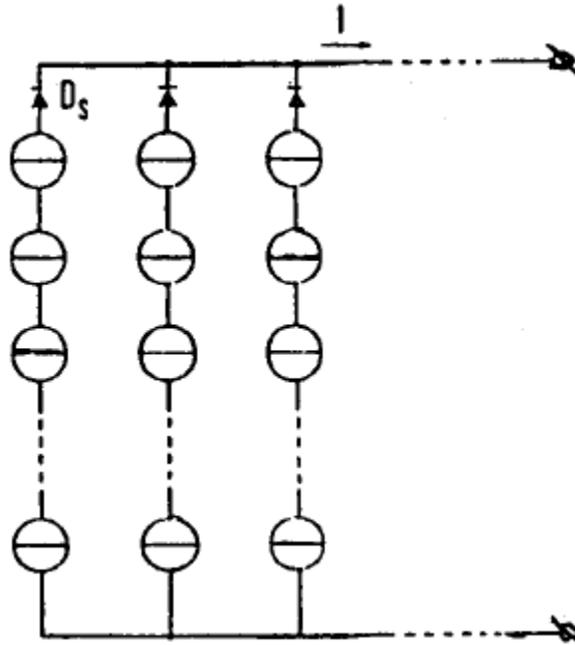
Figure 9 Protection Diode series connected to the strings in parallel.

This protection is anyway not acceptable for the parallel of single cells since the voltage drop across the diode is of the same order of the generated voltage, but it is applicable in case of strings composed of several cells in series.

Chapter 2: Photovoltaic Module

2.1 Structure of a PV Module

A PV module connects several solar cells encapsulated in a protective material shown in Figure 10. The main reason for connecting solar cells into a module is to increase the power output, ranging from a couple of watts to several hundred watts. To increase the power output, even more, several PV modules can be connected into a PV array, which can achieve a power output of a few hundred watts to several megawatts. [3], [4], [5].
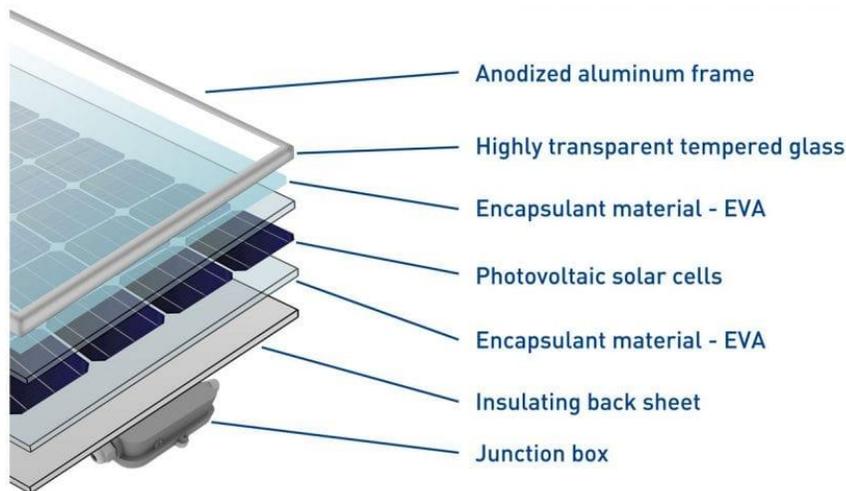
Figure 10 Typical design of conventional PV module

1. Photovoltaic solar cell: is main component that have the function to catch the sunlight and convert it into electricity. Crystalline cells can be monocrystalline or polycrystalline, according to their manufacturing process. The key technical characteristics are size, color, number of busbar and the conversion efficiency.

15

2. Front glass: is the heaviest part of the photovoltaic module and it has the function of shielding and ensuring robustness to the entire photovoltaic module, preserving a high transparency. The thickness of this layer is normally 3.2mm but it can range from 2mm to 4mm depending on the type of glass chosen. It is essential to pay attention to features such as quality of hardening, spectral transmittance and light transmittance. For photovoltaics, some special glasses have been studied with a special pattern on their surface ensuring a greater degree of light trapping. Selecting carefully the glass, checking these features or adding antireflective layers, can bring an overall improvement of the efficiency of the module.

3. Encapsulant material: One of the most essential materials is the encapsulant, which acts as a binder between the various layers of the PV panel. The most common substance used as an encapsulant is EVA – Ethylene vinyl acetate.

4. Back-sheet: The term back sheet exactly means the sheet on the back. It is made from a plastic material that has the function to electrically insulate, protect and shield the PV cells from weather and moisture. This sheet is usually white in color and is sold in rolls or sheets. There are versions that can be different in thickness, in color and in the presence of materials for a greater shielding or for a higher mechanical strength.

5. Junction box: The junction box has the purpose of bringing the electrical connections of the PV module outside. It comprises the protection diodes for shadows and the cables for the connection of the panels in the field

6. Frame: One of the last parts to be manufactured is the frame. It is generally made with aluminum and has the function to ensure strength and a practical and safe coupling to the photovoltaic module.

Lastly, it is significant to mention that the global efficiency of PV-module which is usually lower than that of a single solar cell since there are many supplementary losses that are introduced with the production of the module. In particular, the overall efficiency can be given by the following formula:

$$\eta_{module} = \eta_P \eta_{sc} \eta_T \eta_{MIS} \eta_{IM} \qquad \text{Equation 7}$$

16

- η_P, is the filling efficiency which considers the inactive frontal surface that cannot be exploited for the conversion of the solar radiation into electricity. This loss is related to the fact that when connecting the solar cells, it is not possible to avoid some inactive spaces.

- η_{sc}, is the typical conversion efficiency of a solar cell without considering the EVA or the glass layer.

- η_T, the absorption losses caused by the glass cover materials.

- η_{MIS}, the intrinsic mismatch of module, since they are made of solar cells connected usually in series.

- η_{IM}, for the non-homogeneity of the incident radiation over the module surface.

2.2 Standard Test Conditions (STC)

STC stands for "Standard Test Conditions" and are the industry standard for the conditions under which a solar panel are tested. By using a fixed set of conditions, all solar panels can be more accurately compared and rated against each other. There are three standard test conditions which are:

• Irradiance of 1000 $W \cdot m^2$

• Cell Temperature of 25 $°C$

• Air Mass AM 1,5

2.3 Nominal Operating Cell Temperature (NOCT)

The standard Nominal Operating Cell Temperature (NOCT) is defined in the IEC/EN60904. It is a testing standard geared to the operational conditions of solar cells, defined as the temperature reached by open circuited cells in a module under the following environmental conditions:

• Irradiance of 800 $W \cdot m^2$

• Wind speed of 1 $m \cdot s^2$

17

• Air temperature of 20 °C

NOCT establishes the following relation between the ambient air temperature and the cell temperature:

$$T_c = T_a + \frac{NOCT + T_{a,NOCT}}{G_{NOCT}} * G$$

<div align="right">Equation 8</div>

Where:

• T_c is the cell temperature (°C)

• T_a is the air temperature (°C)

• $T_{a,NOCT}$ is the air temperature at NOCT (°C)

• G is the irradiance (W · m^2)

• G_{NOCT} is the irradiance at NOCT

2.4 Single Diode Model

PV performance model is derived from an equivalent circuit of a solar cell, which consists of a current source, a diode, and two resistors, as shown in Figure 11.

The current source I_{ph} embodies charge carrier generation in the semiconductor layer of the PV cell caused by occurrence radiation. The shunt diode represents recombination of these charge carriers at a forward-bias voltage (V+I·R$_S$). The shunt resistor R_{sh} signifies high-current paths through the semiconductor along mechanical faults and material dislocation. The series resistor Rs exemplifies series resistance in the outer semiconductor regions, mainly at the interface of the semiconductor and the metal contacts.
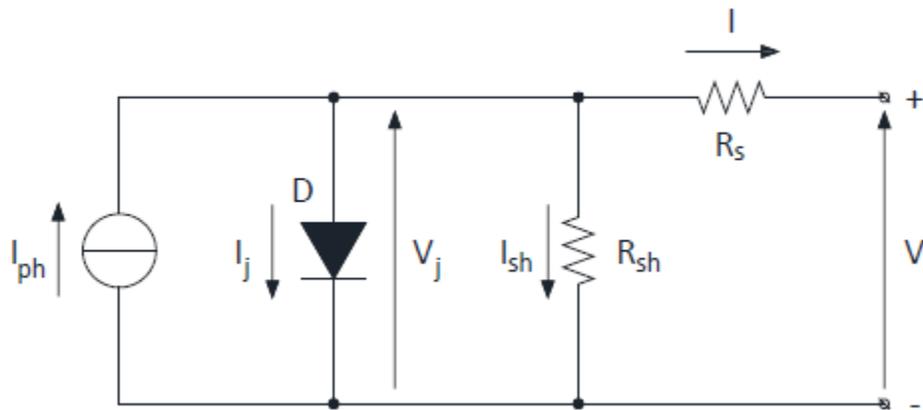
Figure 11 Equivalent circuit of a photovoltaic solar cell used in the five-parameter model. (Source PV Education)

An important parameter for defining the cell is introduced. The fill factor FF is the ratio of the actual maximum obtainable power to the product of the open circuit voltage and short circuit current. This is a key parameter in evaluating performance.

$$FF = \frac{V_{MPP} * I_{MPP}}{V_{OC} * I_{SC}}$$

Equation 9

Where:

- The numerator defines the point of maximum power (W)
- V_{MPP} is the MPP voltage (V)
- I_{MPP} is the MPP current (A)
- V_{OC} is the open circuit voltage (V)
- I_{SC} is the short circuit current (A)

A solar cell with a higher voltage has a larger possible FF. The FF improves for high values of R_{sh} and for low values of R_{S}. On the one hand, the parallel resistance is related to the slope of the I-V curve around I_{sc}. The series resistance, on the other hand, is related to the pendant in V_{oc}. The higher the value that the fill factor assumes, the better the cell quality. In this case, R_{s} and R_{sh} have a not very significant influence. The influence of the resistances on the I-V curve can be seen in the Figure 12.

19
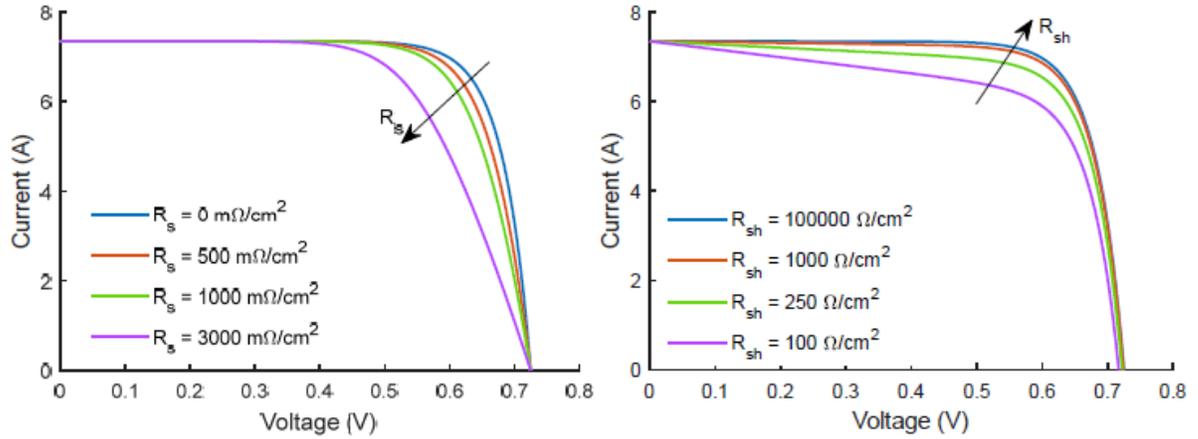
Figure 12 Dependence of the I-V curve on the parallel and series resistances

The circuit shown in the Figure 11 can be solved with respect to current and with respect to voltage. In the first case the following calculation is obtained.

$$I = I_{ph} - I_j - I_{sh}$$
Equation 10

Where:

- I is the cell output current (A)
- I_{ph} is the photogenerated current (A)
- I_j is the current in the diode (A)
- $I_{sh} = \dfrac{V_j}{R_{sh}}$ is the current in the parallel resistance (A)

$$I_{ph} = q_e * N_{ph} * S$$
Equation 11

Where:

- $q_e = 1{,}602 \cdot 10^{-12}$ C is the charge of the electron
- N_{ph} is the number of incident photons in $(m^{-2} \cdot s^{-2})$
- S is the surface of the cell (m^2)

$$I_j = I_o * \left(e^{\frac{q_e * V_j}{n * k_B * T_c}} - 1 \right)$$

Equation 12

Where:

- I_j is the reverse saturation current of the diode (A)
- V_j is the voltage on the diode (V)
- n is the ideality factor of the diode
- $k_B = 1{,}38 \cdot 10^{-23}$ J $\cdot$ K^{-1} is the Boltzmann constant
- T_c is the p-n junction temperature (K)

The formula (2.9) is obtained by combining the previous ones.

Tension can be expressed with the following formulas.

$$V = V_j - R_s * I$$

Equation 13

Where:

• V is the cell output voltage (V)

Obtaining V_j from equation (12) and replacing in (13)

$$V = \frac{n * k_B * T_c}{q_e} * \ln\left(\frac{I_{ph} + I_o - I - I_{sh}}{I_o}\right) - R_s * I$$

Equation 14

The open circuit voltage is obtained when $I = 0$

$$V_{oc} = \frac{n * k_B * T_c}{q_e} * ln\left(\frac{I_{ph} + I_o - I_{sh}}{I_o}\right)$$

Equation 15

Voltage and current equations can be combined substituting equation (13) in (12)

21

$$I = I_{ph} - I_o * \left(e^{\frac{q_e * V + R_S * I}{n * k_B * T_c}} - 1 \right) - \frac{V + R_s * I}{R_{sh}} \qquad \text{Equation 16}$$

The short circuit current is obtained when $V = 0$

$$I_{SC} = I_{ph} - I_o * \left(e^{\frac{q_e * R_S * I}{n * k_B * T_c}} - 1 \right) - \frac{R_s * I}{R_{sh}} \qquad \text{Equation 17}$$

2.5 Main Photovoltaic Technologies

Photovoltaic (PV) systems directly convert sunlight into electricity. The PV effect is the process from which light (photons) is converted into electric current [14]. Different PV technologies have different efficiencies. There are 3 main classes of photovoltaic semiconductor technologies:

1.Crystalline silicon cells: lead the world PV market, reporting for nearly 90 percent in 2013. Although single crystalline cells account for most PV panels, there are a few types of silicon PV technologies on the market today.

- single crystalline silicon (c-Si),
- multicrystalline (mc-Si)
- silicon heterostructure.

2.Thin film technologies: are described by one or more thin layers of photovoltaic material (at least 10 times thinner than crystalline silicon technologies) placed onto glass, plastic, metal, or another surface. As a result, thin film cells are more flexible and weigh less. They can be incorporated into buildings, including as photovoltaic material laminated onto windows. Thin film solar panels within panes of glass are used in some of the largest PV power plants. Some thin film cell technologies include:

- Amorphous silicon (a-Si) and other thin film (TF-Si)
- Cadmium telluride (CdTe)
- Copper indium gallium deselenide (CIS or CIGS)

- Dye-sensitized solar cells (DSC)
- Single crystalline gallium arsenide (GaAs)

3. Multijunction cells: consume light at different wavelengths more efficiently than crystalline silicon cells through multiple stacked layers of semiconductors. Although more efficient at translating sunlight into electricity, they are currently less efficient economically due to their complexity and subsequent manufacturing costs. This price has reduced their application mainly to the aerospace industry, which is uniquely willing to pay more for their higher efficiencies.

Monocrystalline Solar Panel   Polycrystalline Solar Panel   Thin-Film Solar Panel
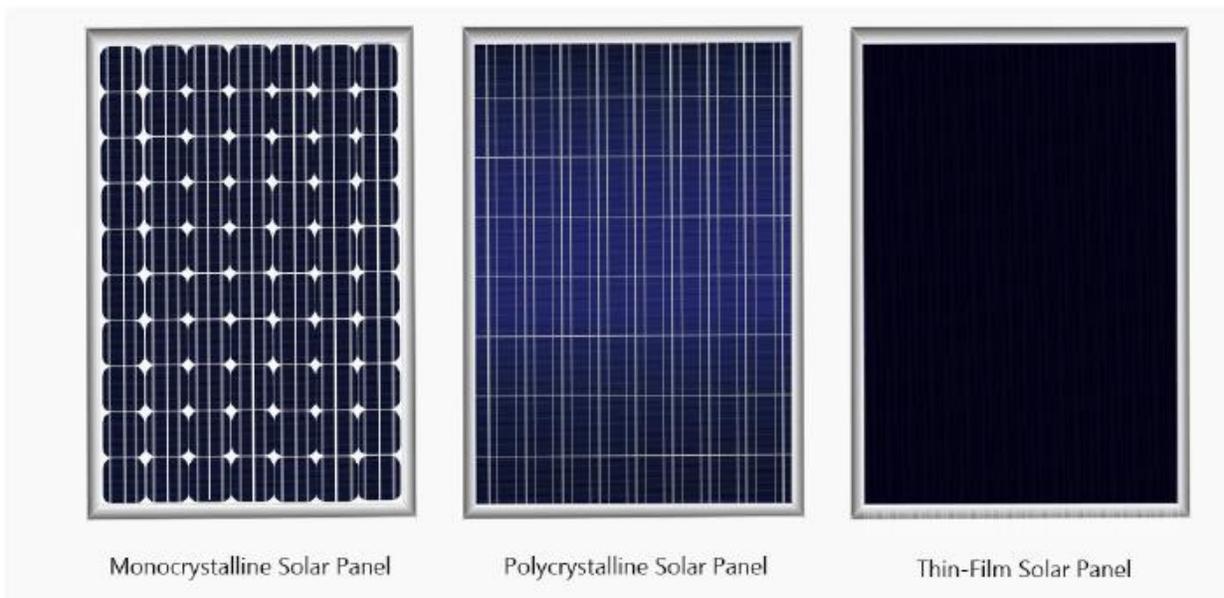
Figure 13 Main P-V module technologies (Source: Solar Magazine)

2.5.1 Monocrystalline Silicon Solar Cells

Crystalline silicon PV cells are the most common solar cells used in commercially accessible solar panels, representing more than 85% of world PV cell market sales in 2011. Crystalline silicon PV cells have laboratory energy conversion efficiencies of over 25% for single-crystal cells and over 20% for multi-crystalline cells. Nevertheless, industrially manufactured solar modules currently accomplish efficiencies ranging from 18%–22% under standard test conditions. A monocrystalline solar panel is a solar panel involving monocrystalline solar cells. These cells are made from a cylindrical silicon ingot grown from a single crystal of silicon of high purity in

23

the same way as a semiconductor. The cylindrical ingot is sliced into wafers forming cells. To maximize the utility of the cells, the circular wafers are wire cut to an octagonal-shaped wafer. These cells have a unique look because of their octagonal shape. These cells also have a uniform colour.

A standard industrially produced silicon cell offers higher efficiencies than any other mass-produced single-junction device. Higher efficiencies reduce the final installation cost because fewer solar cells need to be produced and installed for a given output. In addition, crystalline silicon cells reach module lifetimes of 25 years and display small long-term degradation.

2.5.2 Polycrystalline Silicon Solar Cells

Polycrystalline solar panels normally have lower efficiencies than monocrystalline options, but their advantage is a lower price point. Additionally, polycrystalline solar panels tend to have a blue color instead of the black shade of monocrystalline panels.

Polycrystalline solar panels are also made from silicon. Though, instead of using a single crystal of silicon, manufacturers melt many fragments of silicon together to form the wafers for the panel. Polycrystalline solar panels are also referred to as "multi-crystalline," or many-crystal silicon. Since there are many crystals in each cell, there is less liberty for the electrons to move. As a result, polycrystalline solar panels have lower efficiency ratings than monocrystalline panels. The durability is like that of the previous technology, as they should last for more than 25 years.

Chapter 3: Optimization Algorithm

Optimization of algorithms is a favorable tool that can be used to find a good approximation of the optimal value of a specific problem whenever the function describing its behavior is too complex to find an exact analytical solution. When dealing with global optimization problems, the goal is to discover the best solution, according to a specific criterion (objective function), when several local solutions are possible. Due to their many possible applications, optimization algorithms have been the subject of numerous studies. Therefore, there are many optimization algorithms in literature as there is no single algorithm suitable for all problems. The right choice of an optimization algorithm can be crucially important to find the right solution for a given optimization problem

Levenberg-Marquardt Algorithm

The Levenberg-Marquardt algorithm was developed in the early 1960's to solve nonlinear least squares problems [19] [20]. Minimum squares problems arise in the framework of fitting a parameterized mathematical model to a set of data points by reducing an objective stated as the sum of the squares of the errors between the model function and a set of data points. If a model is linear in its parameters, the least square's objective is quadratic in the parameters. This purpose may be diminished with respect to the parameters in one step via the solution to a linear matrix equation. If the fit function is not linear in its parameters, the least squares problem requires an iterative solution algorithm. Such algorithms decrease the sum of the squares of the errors between the model function and the data points through a series of well-chosen updates to values of the model parameters. The Levenberg-Marquardt algorithm blends two numerical minimization algorithms: the gradient descent method and the Gauss-Newton method. In the gradient descent method, the sum of the squared errors is reduced by updating the parameters in the steepest-descent

direction. In the Gauss-Newton method, is the quantity of the squared errors is reduced by assuming the least square's function is locally quadratic in the parameters and finding the minimum of this quadratic. The Levenberg-Marquardt method acts more like a gradient-descent method when the parameters are far from their optimal value and acts more like the Gauss-Newton method when the parameters are close to their optimal value.

The characteristic equation of the Levenberg Marquardt method is:

$$[J(P)^T J(P) + \lambda I]\delta = J(P)^T * (y - \hat{y}(p)) \qquad \text{Equation 18}$$

Where:

- J it is the Jacobian matrix
- p is the vector of n parameters (variables to be optimized for the algorithm)
- λ damping parameter
- I it is the identity matrix
- δ is the length of the calculated step
- y independent variable
- $\hat{y}(p)$ model curve

The value of λ describes the behavior of the algorithm:

- For small values of λ the algorithm approaches the Gauss Newton Method.
- For high values of λ the algorithm approaches the Gradient Search Method.

The value of λ is adapted to each iteration, increasing it if the previous iteration produced is limited reduction in the objective function, or diminishing it in case of rapid decrease.

Chapter 4: Data Acquisition System

This chapter explains the way the I-V curve of the PV modules are measured. Firstly, the *I-V* curve measurement principle will be described. Then, the measurement system adopted will be explained in detail and the evaluation of the measurement uncertainty will be computed in the last segment.

4.1. I-V Curve Measurement Method

An I-V curve measurement is executed by applying a series of voltages to the device. At each voltage, the current flowing through the device is measured. The provided voltage is measured by a voltmeter connected in parallel to the device, and the current is measured by an ammeter connected in series. The measurement can also be performed using a source measure unit, a device capable of concurrently supplying voltage and measuring current with high accuracy. The Figure 14 shows the schematic of the circuit diagram of the IV diagram.
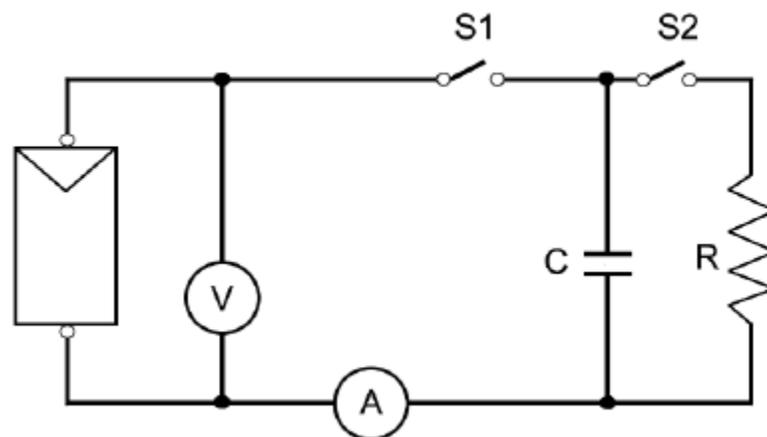
Figure 14 Basic schematic of I-V curve measurement system.

The circuit consist of a capacitive load (C) connected to the terminals of the PV module through a breaker (S1). A secondary discharge circuit is added in parallel, which consist of a discharge resistance (R) and a second breaker (S2). Lastly, a voltmeter and an ammeter are used to measure the voltage and the current, respectively, during the charging process [23].

According to technical specification generally recognized, the proper tracking of an appropriate I V curve implies measuring at least 50 points I-V in a process lasting a time ranged between 120 and 300 ms. In this way, the variation in weather conditions does not affect the measure of the I-V curve.

Capacitive load

The second evaluating method is based on biasing the module by a large capacitor, which is charged while the former moves from short circuit to open circuit. Mentioning to the figure 15 at the starting of the measurement the capacitor is short-circuited and when the S2 switch is opened and the S1 is closed its loading starts. As the charge of the capacitor increases, current drops and voltage rises. When the charge is completed, the current supplied by the module becomes zero and the open circuit condition is achieved [24]. The charging transient of a capacitor is the simplest method that can be used to trace the *I-V* curve. In fact, the charging time of the capacitor can be defined by the following differential equation:

$$i(t) = C * \frac{dv(t)}{dt}$$ Equation 19

Where:

- $i(t)$ is the current (A) flowing in the capacitor
- C is the measured capacitance (F)
- $v(t)$ is the voltage (V) across the capacitor
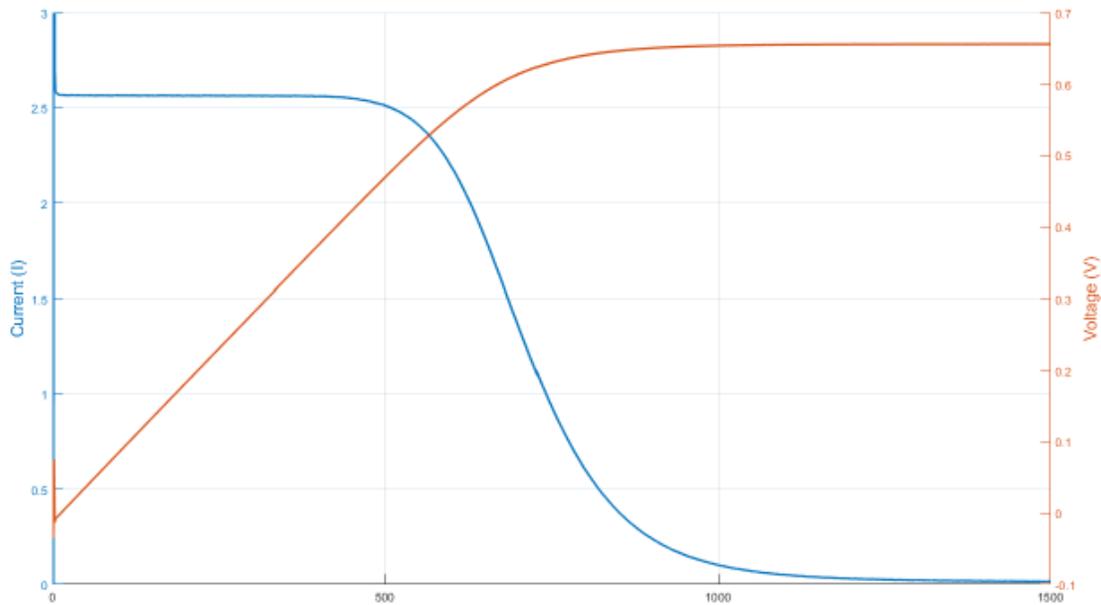
Figure 15 Charging transient of a capacitor connected to a PV module.

The time evolution of the two quantities can be observed in Figure 15. The evolutions of voltage and current follow an asymptotic tendency. Thus, in theory the capacitor will never reach the open circuit voltage. For this reason, usually the transient is considered completed when voltage reaches 99.33% of the open circuit voltage.

Furthermore, if a full charge transient from short circuit to open circuit is considered, it is possible to estimate the charging time with the following equation.

$$t_c = \frac{C}{A} * \frac{V_{OC} * N_S}{I_{SC} * N_P}$$ Equation 20

Where:

- t_C is the charging time of the capacitor (s)
- $A = 0{,}55$ is the proportionality factor (-)
- V_{OC} is the open circuit voltage (V)
- I_{SC} is the short circuit current (A)

- N_S is the number of cells in series (-)
- N_P is the number of cells in parallel (-)

A precise estimation of the charging time is vital to correctly set the measuring system. For this reason, this parameter needs to be estimated before the acquisition of the I-V curve. The assessment can be achieved by manipulating the relationship between the charging time and atmospheric conditions (irradiance and temperature) since they have a great influence on the values of short circuit current and open circuit voltage.

4.2 Measurement System

The measurement system used for the data acquisition was placed in the flat roof of the Higher Technical College of the University of Jaén [19] as shown in Figure 16.

Figure 16 Higher Technical College of the University of Jaén

The system is designed to measure the electrical parameters of a single PV modules, along with the atmospheric conditions. This information is useful to analyze the electrical behavior of the modules under different outdoor conditions. The experimental setup can measure the *I-V* curves automatically and constantly, with the possibility of setting the lapse of time between each measurement (e.g., 2 - 5 min). From the measure of the *I-V* curve for each module it is possible to obtain the most important points, such as V_{oc}, I_{sc} and P_{max}.

The characteristics for the fixed tracker systems is represented in blue and in orange respectively.
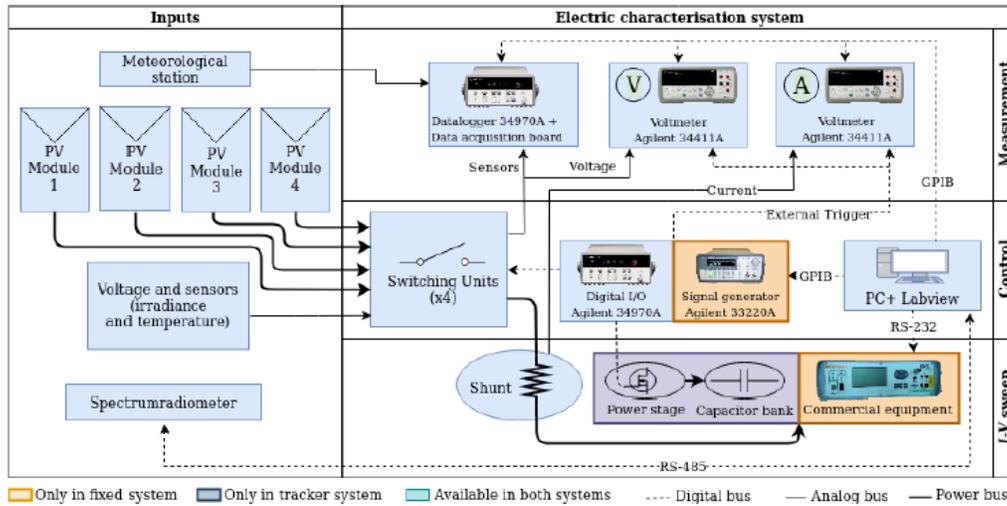
Figure 17 Measurement system schematic highlighting the parts for fixed system.

In figure 17, it is possible to identify two main blocks. The first one the input column comprises of the meteorological stations, the temperature and irradiance sensors. The second one is the electrical characterization system. Specifically, it is possible to identify the instrumentation used to record the measurements performed by the various sensors, as well as two multimeters used to record voltage and current.

The data acquisition procedure is completely automatic and iterative. The first step of the procedure consists of the configuration of the initial conditions, which involves the manual configuration of the electrical features of the PV modules as well as the selection of the electrical parameters to measure and the time step between each measurement (e.g., 2-5 min). The working window is defined by some upper and lower limits for the irradiance value.

The iterative procedure consists of recording of the atmospheric conditions. For the acquisition of the atmospheric parameters a wide range of sensors have been installed on the system. The sensors can measure multiple meteorological data such as ambient temperature and irradiance.

4.2.1 Measurement of Module Temperature (T_C)

Module temperature (T_C) a resistance temperature detector (RTDs) of the Pt100 type with 4-wire connection is adopted. This sensor consists of a probe made of platinum (Pt) with a 100 Ω resistance at 0 °C. The temperature coefficient "α_{Pt100}" of this sensor is 0,00385 $\Omega \cdot \Omega^{-1} \cdot K^{-1}$. This

31

coefficient describes the linear approximated characteristic of the probe resistance variation with temperature:

$$\alpha_{Pt100} = \frac{R_{100} - R_O}{100 * R_O}$$

Equation 21

Where:

- α_{Pt100} = 0,00385 $\Omega \cdot \Omega^{-1} \cdot K^{-1}$ is the temperature coefficient
- R_{100} is the sensor resistance at 100 °C measured (Ω)
- R_{100} is the sensor resistance at 0 °C measured (Ω)

The temperature value is calculated by a measurement of the resistance of the Pt sensor in a 4-wire configuration as shown in Figure 18. A 4-wire measurement is precise and unaffected by the length of the laboratory wires. The datalogger is set properly to make the conversion. The selected probe works for temperature ranged between -50 °C and +150 °C.

Figure 18 The Pt100 Temperature probe

4.2.2 Measurement of Irradiance (G)

The global in-plane irradiance (GTI or G) represents the global solar power per unit of area received by a surface with an azimuth and zenith angle. Essentially the GTI is composed of the direct and diffuse radiation components. The GTI is measured by a Kipp and Zonnen CMP11

32

pyranometer, as in Figure 19. The instrument is placed coplanar with the modules under study. The pyranometer provides an output voltage signal proportional to the incidental irradiance. Moreover, this voltage signal can be converted in irradiance units with the calibration constant. This calibration constant came from the manufacturer calibration or from external calibration in an accredited laboratory (i.e., CIEMAT in Madrid). The output signal from the pyranometer is measured with the datalogger.

Figure 19 Picture of the pyranometer

4.2.3 Measurement of Wind Speed

A Young 05305VM anemometer in Figure 20 is used to measure the wind speed (WS) and wind azimuth direction (WD). The tool requires two output-voltage signals linearly proportional to the computed WS and WD. The datalogger is used to measure those signals.

Figure 20 The Young 05305VM anemometer.

33

4.2.4 Measurement of the atmospheric pressure (p_{amb})

Vaisala BAROCAP PTB110 barometer in Figure 21 is used to measure the atmospheric pressure (p_{amb}). The device provides as output a voltage signal proportional to the atmospheric pressure.

Figure 21 The Vaisala BAROCAP PTB110 barometer.

4.2.5 Measurement of the ambient air temperature (T_a) and relative humidity (RH)

The Young 41382VC temperature and relative humidity probe as in Figure 22 is used to measure the ambient air temperature (T_a) and relative humidity (RH). The tool provides two output-voltage signals linearly proportional to the measured air temperature and relative humidity. The datalogger is used to measure those signals.

Figure 22 The Young 41382VC temperature and relative humidity probe.

4.2.5 Measurement of the triband irradiance

The Tri-band Spectro-heliometer from IES-UPM, shown in Figure 23, evaluates the irradiance in the spectral zones relating to the top, middle, and bottom sub-cells of a lattice-matched GaInP / GaInAs / Ge triple-junction solar cell. This device is helpful to achieve

34

experimental campaigns about concentrator photovoltaics. The sensor gives an output a voltage signal linearly proportional to the band irradiance calculated by the datalogger. Only the solar tracker is outfitted with this instrument.
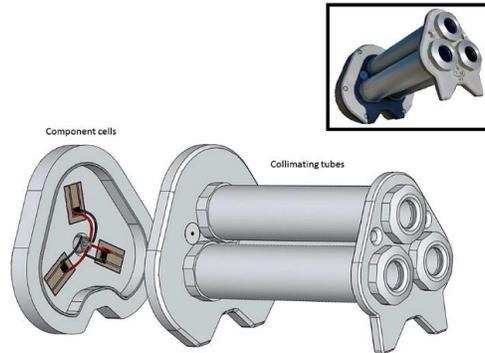
Figure 23 Tri-band Spectro-heliometer from IES-UPM [27]

4.2. Automatic Curve Tracer for PV Modules

The "tracker system", uses a BSQ D150/6 Solar 2-axes tracker. This system is constructed with a 2-axis solution to carry the PV module always perpendicular to the sun light. The tracker is constructed to carry out experiments on concentration solar energy with a maximum misalignment of ±0,5°. In this manner, the angular reflection losses are avoided. Additionally, the system functions as described in 4.1. The system integrates the instruments mentioned earlier, that are module temperature probe, pyranometers. Additionally, the two multimeters are synchronized by the Agilent 34970A datalogger that provides a trigger signal through the Agilent 34907A Digital Multifunction Module. Furthermore, the datalogger directs the connection of one of the four modules under test by the switching units in Figure 24 [28].

Academic year 2020/2021

Figure 24 The tracker system on the left the external part, on the right the internal equipment.

Furthermore, the tracker system contains a capacitive load for tracing the *I-V* curves, as shown in Figure 25. This load principally consists of three elements:

- The first one is the electrolytic capacitor with a capacitance of 47 mF and a maximum voltage of 100 V.
- The second one is the discharge resistance which is used to discharge the capacitor.
- Lasty a voltage generator used to negative pre-charge the capacitor and to get the short circuit current.

Figure 25 View of the inside of the capacitive load

The working principle of the Agilent 34970A datalogger regulates the charge and discharge of the capacitive load using relays as shown in Figure 26. Initially, the datalogger terminates only SW7, shown in Figure, to negative pre-charge of the capacitor. This procedure is necessary to get the short circuit current point. Moreover, a diode is essential to avoid problems associated to the internal diode of the solid-state relays. Further information can be found in [28].
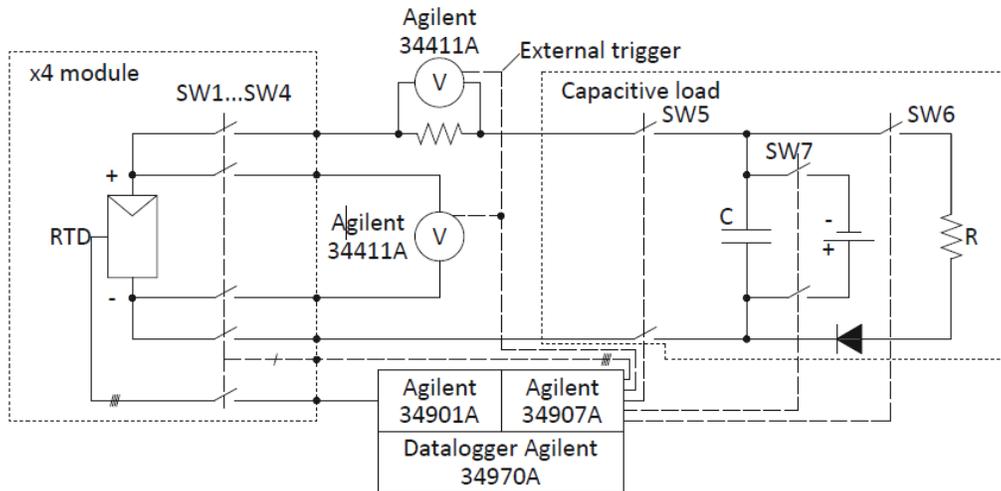
Figure 26 Electrical scheme of the tracker system.

Considering the Figure 26, the datalogger opens SW7 and then it closes SW5. This system of instructions connects the PV module to the capacitor load C. Afterwards, the multimeters can acquire the voltage and current synchronously. The data acquisition is done in a specific time referred to the capacitive load properties. The approximation of the charging time (t_c) is important to go through the timing requirement according to 4.1. This evaluation is done according to eq. (4.2). The time among two samples is settled accurately for acquiring the entire curve with enough points. Finally, the datalogger reopens SW5 at the end of the transient and it closes SW6 to discharge the capacitor on a resistor for the next acquisition.

The entire system is controlled with LabVIEW software on a devoted PC. The instruments are attached to the PC through GPIB connections, excluding for the spectroradiometer that needs a RS485-RS232 serial connection. Figure represents the LabVIEW graphical user interface of tracker system (*I-V*-curve tab).

37
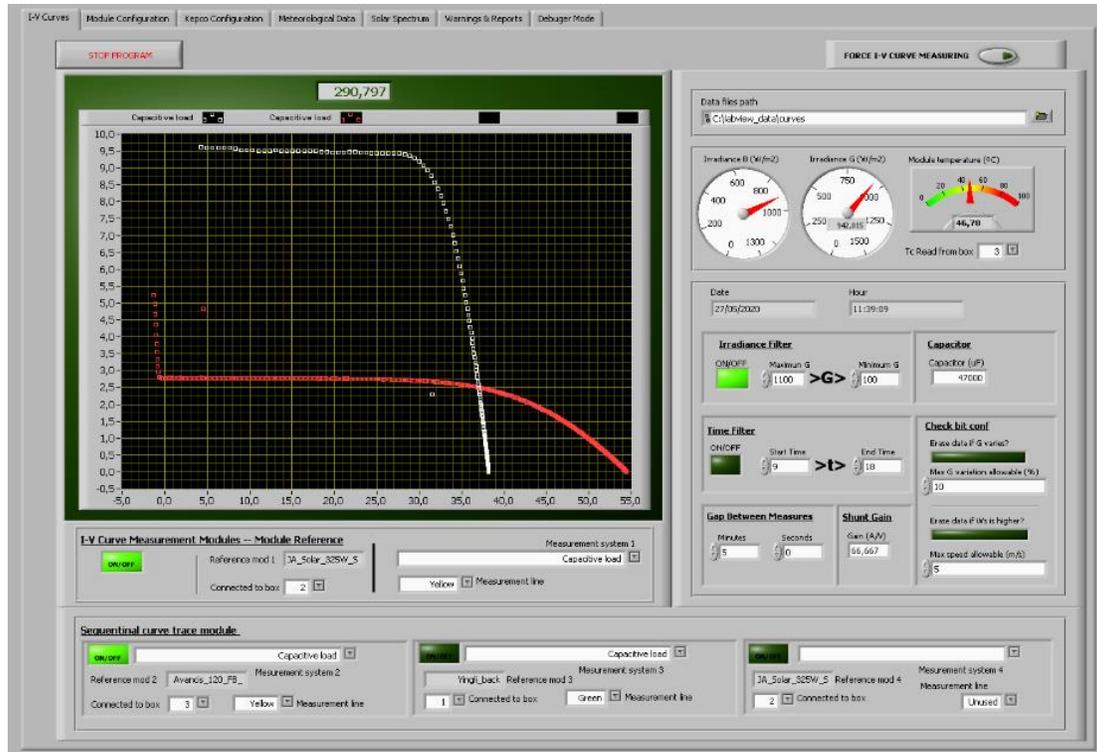
Figure 27LabVIEW graphical user interface of tracker system (I-V-curve tab).

The LabVIEW software process is represented in the flowchart Figure. Besides, the software is designed to offer the user with additional facilities to configure the measurement process. Furthermore, the graphical interface demonstrates in real time the attained data such as the *I-V* curves, the value of irradiance and temperature. The software's user interface is shown in Figure. The program saves as output the data from various sensors and devices in one "CSV" file for each measurement. The output CSV file is organized with one column for each measured quantity. All columns contain 1500 values, creating a matrix. All 1500 values are equal in case of a physical quantity with a single point (i.e., temperature, irradiance, etc.).
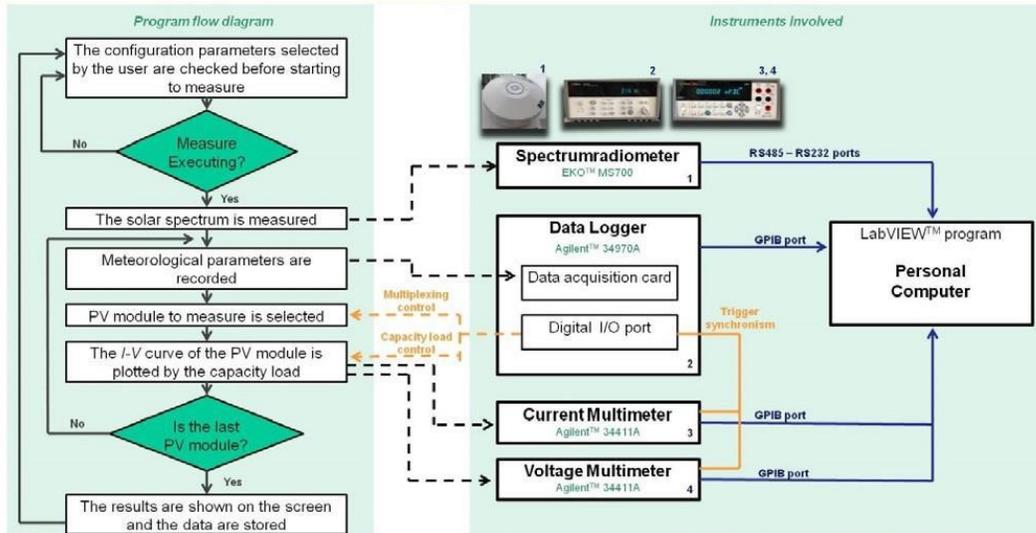
Figure 28 LabVIEW measurement control software flowchart.

Chapter 5: Analysis of Experimental Data using GUI

In this chapter the MATLAB software is going to be explained. The program is designed with the use of MATLAB App Designer tool to achieve a simpler interface. The application intends of processing automatically large amount of data acquired by the measurement systems. The graphical user interface (GUI) is distributed into several tabs. Each tab handles individually one section of the process. This division is done in order to have the chance of looking at the partial result of each part. Also, this subdivision allows to reprocess part of the interface to execute other tasks. The next four chapters deal individually each GUI's tab. Figure 27 shows the flows of these four tabs.
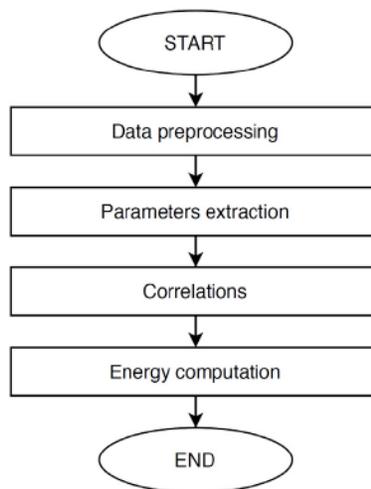
Figure 29 Flowchart of the four steps of the GUI.

First, the data preprocessing will be described. This step consists in the examining and filtering of the raw data. Then, the parameters extraction procedure will be explained. This step comprises in the search with the optimization algorithms, used to find the parameters of the model that explains the system. After that, the extraction of correlation coefficient will be explained. This

40

step consists in the quest for irradiance and temperature trends. Last, the energy estimation will be done. This step consists in the approximation of power in a bigger set of data, in order to authenticate the correlation model.

The GUI and the software are established by the support of the following Math-Works products and toolboxes:

- MATLAB
- App Designer
- Curve Fitting Toolbox
- System Identification Toolbox
- Statistics and Machine Learning Toolbox
- Parallel Computing Toolbox
- Predictive Maintenance Toolbox
- Signal Processing Toolbox

The helpful terms in the App Designer category are defined in the MATLAB catalogue and here are mentioned:

- "Button" is a component that indicates when the user presses and releases it
- "Check Box" is a component representing the state of a preference or option
- "Drop Down" is a component that allows the user to choose an option or type in
- the text
- "Text Area" is a component essential to enter for entering multiple lines of text
- "Tab Group" is a container for grouping and managing tabs
- "Panel" is a container for grouping other components together
- "Switch" is a component indicating a logical state
- "Lamp" is a component that reporting the state using color
- "Edit Field" is a component that allows the user to type numeric/text values
- "Button Group" is a component that allows the user to choose one button from the set
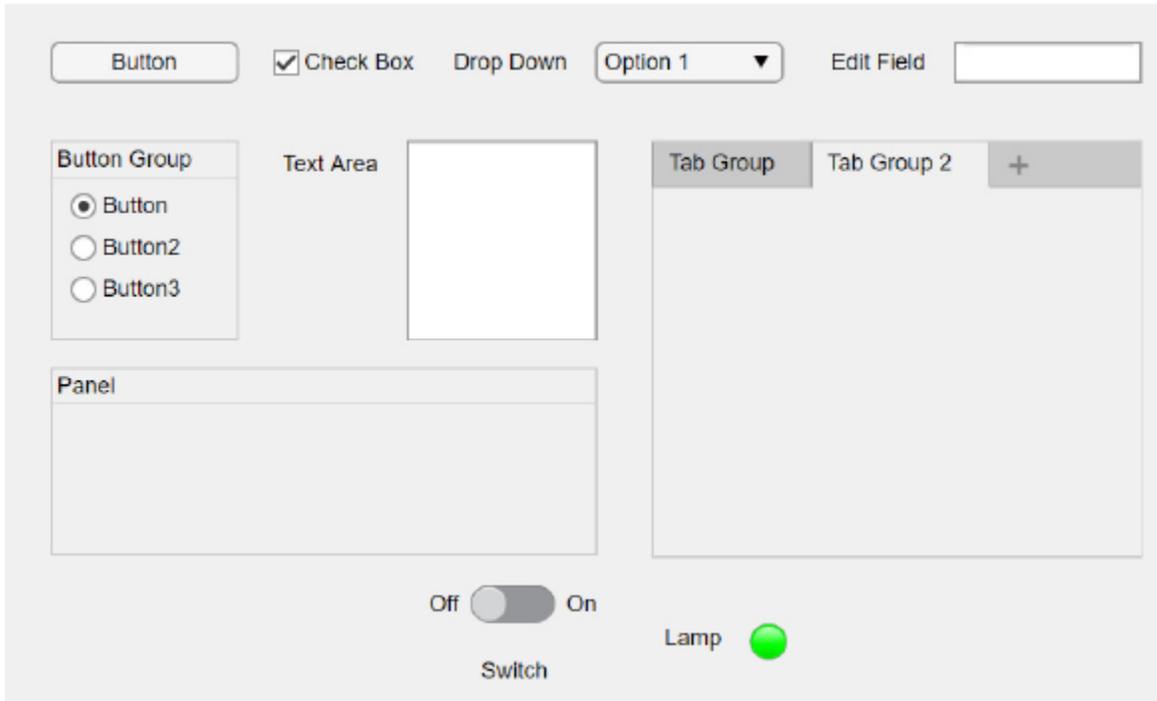
Figure 30 MATLAB App Designer helpful components

Chapter 6: Step 1-Data Preprocessing

The data preprocessing contains reading CSV files from the measurement system while removing the unrealistic measurement automatically. Later, some filters are applied to fulfill this task. The graphical interface is constructed to include all the necessary settings in the utmost intuitive sense. Figure 29 represents the interface when the program opens.
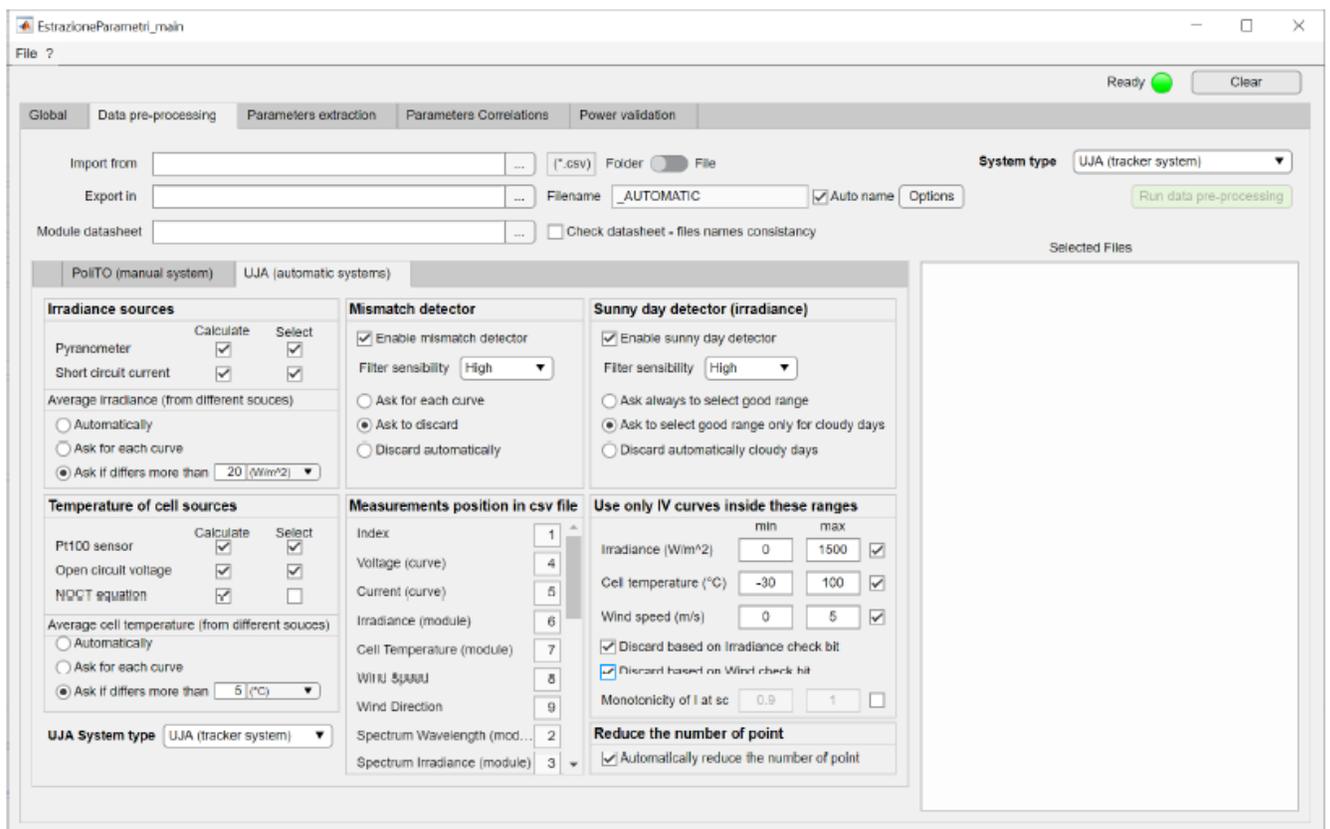
Figure 31 The graphical user interface tab for the preprocessing data task.

43

Figure 29 can be divided into two sections. The first section demonstrates the import and export settings. whereas the second is "UJA (automatic system)". And the third section is the, "PoliTO (manual system)". However, this section is not explained because this thesis only processes data obtained from university of Jean.

6.1. Import and Export Settings

In the data preprocessing tab, the import and export settings are situated in the upper part of the interface as shown in Figure 30.
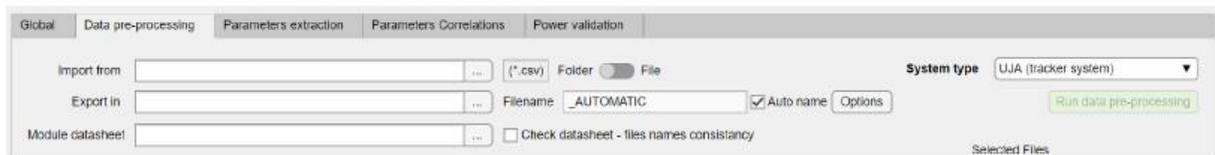
Figure 32 The import and export settings in the graphical user interface

The first edit field permits the user to choose the file path. The input selection can be done in two ways whether to select an entire folder or to select multiple files. The UJA system accepts only the CSV files for the importation.

On the other hand, the exportation column allows the user to select the data export folder in the preferred format. It can be made by simply clicking the "Options" button adjacent to exportation column. The options button will open a new window as shown in the Figure 31.
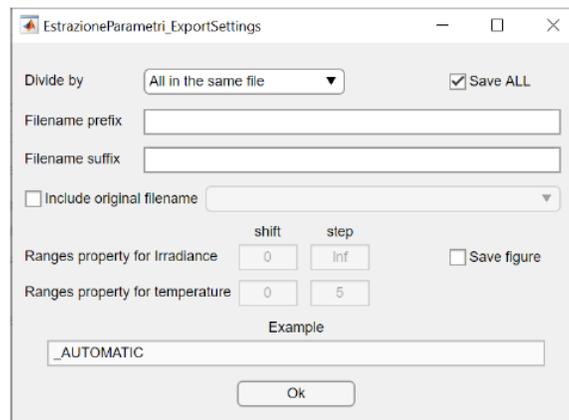
Figure 33 The window for selecting the saving properties

44

Export settings in the list box allows to divide the data in various ways. There are various types of data divisions: "All in the same file", "Divide by days", "Divide by months", "Divide by years", ''Divide by irradiance", "Divide by temperature (module)", "Divide by irradiance and temperature (module)". The selection of saving data by irradiance and/or temperature comprises a further requirement called "the ranges property". At this point, the user must insert two values for quantity: a preliminary shift value from zero and a step value. The ranges division is formed only between the minimum and maximum rounded values of the quantity. An example for the irradiance case with shift $= 25$ and step $= 50$ means the division of the irradiance in the ranges (0-25], (25,75], (75,125], …, (975,1025]. If there is only one measure with $G = 1000$ W $\cdot$ m^{-2}, the ranges division results in (975,1025].

Very similar logic is applied to the module temperature classification. In the same options window, there are two optional edit fields that permits the user to insert a prefix and a suffix to the name of the output data. Furthermore, in the final file name, the user can also decide to include the original filename of the CSV file. Lastly, two checkboxes can be seen. The "Save ALL" checkbox keeps a copy of all loaded information before applying the filters. Whereas the "Save figure" checkbox saves the figures of the day irradiance and the I-V and P-V curves of each acquisition. The third edit field allows the user to select the Excel datasheet files with the corresponding format as shown in Figure 32.

	Value	Unit of measuremen	Notes
module name	kyocera_MULTI	-	Must finish with '_'
$P_{max,STC}$	141.1	W	Power MPPT in STC conditions
$I_{sc,STC}$	8.64	A	Short circuit current in STC conditions
$V_{oc,STC}$	22.1	V	Open circuit voltage in STC conditions
$\alpha\ (I_{sc})$	0.058	%/K	Coefficiente di temperatura Isc
$\beta\ (V_{oc})$	-0.362	%/K	Coefficiente di temperatura Voc
$\gamma\ (P_{max})$	-0.435	%/K	Coefficiente di temperatura Pmax
NOCT	49.0	°C	NOCT temperature
Ns	36	-	Number of cell in series
Nc	1	-	Number of cell in parallel
Cell dimension	156	mm	
G_{STC}	1000	W/m^2	Irradiance in STC conditions
Tc_{STC}	25	°C	Cell temperature in STC conditions
G_{NOCT}	800	W/m^2	Irradiance in NOCT conditions
Ta_{NOCT}	20	°C	Air temperature in NOCT conditions

Figure 34 The module datasheet of Kyocera KD 135GH- 2PU in Excel.

45

The last element of the import and export settings is the "System type" list box. The user selects the desired measurement system. Like this work is entirely based on the UJA custom system.

6.2. Selection of Sources and Filters

The UJA (automatic system) is positioned in the lower part of the interface. It consists of seven panels all containing settings. These settings will be described in the following work.

Figure 35 The graphical user interface for the preprocessing task- UJA (automatic system).

1. The "Irradiance sources" panel permits the user to select the irradiance sources. The sources can be the pyranometer or the short-circuit current or may be both. In the last case, the user may choose the approach of calculating the average value of the two sources. By selecting methods between "automatically", "semi-automatically" or "manually". These methods define the degree of user intervention. A popup window appears if non automatic case is chosen, shown in Figure 34.
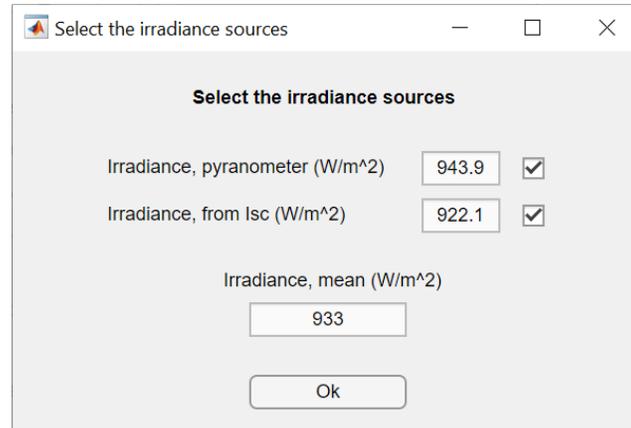
Figure 36 Popup window for manual selection for irradiance.

2. The "Temperature sources" panel permits the user to select the temperature sources to be used. The sources of module temperature are the Pt100 probe, the open circuit voltage and the NOCT equation. The temperature considered is the average value if more than one source can be selected. Similarly, the popup window appears as shown in Figure 35.
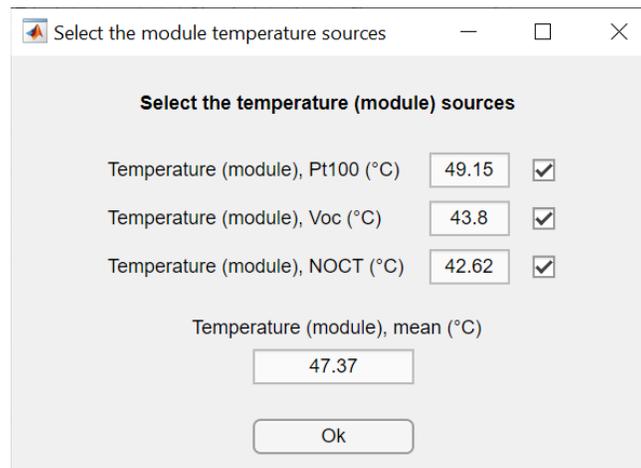
Figure 37 Popup window for manual selection for temperature.

3. The "Measurement position in CSV file" panel indicates the column position for each measured quantity in the CSV file. The position of each quantity is given in three preloaded profiles, two for the tracker system and one for the fixed system. As we have selected the UJA custom system. In this selection the edit fields. If a quantity is not present in the CSV file, a value of "-1" should be written down. Furthermore, it is essential to indicate that a CSV file contains the values of the measurements for an *I-V* curve acquisition.

47

4. The "Mismatch detector" and the "Sunny day detector (irradiance)" panels are made up of three elements. First check box enables the mismatch/sunny day detector. Secondly, the list box allows the user to specify three level of filter's sensibility (high, medium, low). Lastly, the button defines the user to automatically discard the IV curve.

5.The "Use only *I-V* curve inside these ranges" panel is comprised of edit fields for four quantities. These quantities are irradiance, cell temperature, wind, and current monotonicity at short circuit ranges. Besides, this panel includes two check boxes for filtering the data with the irradiance and/or wind check-bits.

6. The "Reduce the number of points" panel includes the check box that enables a reduction in the *I-V* curve points.

Chapter 7: Stage 2- Parameters Extraction

This chapter explains regarding the parameter extraction process is a numeric optimization that help us to solve the system equations linked with the PV cells equivalent circuit. The GUI is created to implement two different PV models and three different extraction algorithms. The two models are the five and seven parameters. The three algorithms are the Levenberg-Marquardt (LM), Simulated annealing (SA), and finally, a third algorithm can be added for future analysis. Summing up, for this thesis only the five parameters model and the LM algorithm will be considered for the elaboration.

7.1 Parameter's Extraction Settings

The tab for the parameter extraction is designed to contain all necessary settings for this operation. Figure 36 shows the interface when the tab is open.
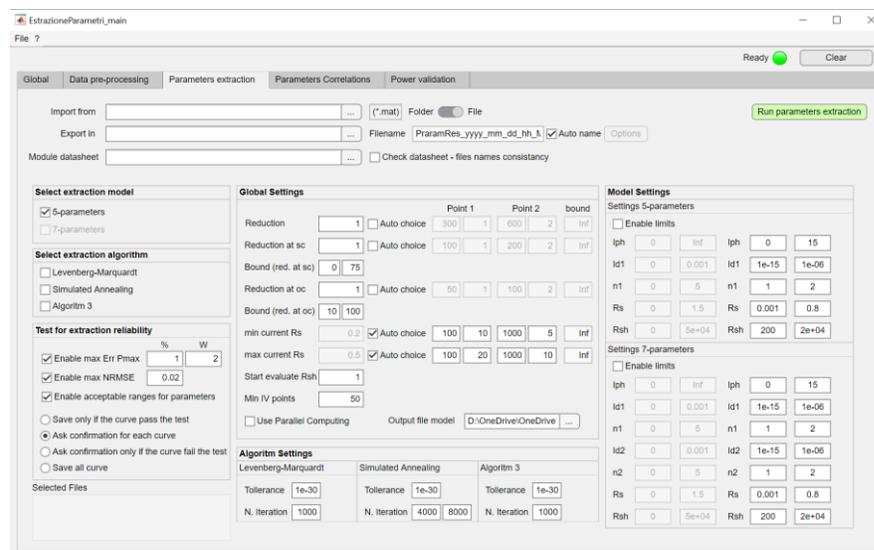
Figure 38 the graphical user interface tab for the parameter's extraction

The import/export section, works exactly same way as the data preprocessing, described in chapter 6.

The parameter's extraction settings are categorized in six panels. These panels will be described starting from the model/algorithm selected up to specific settings. The first panel "Select extraction model", extraction of both models (5 and 7 parameters) is executed automatically and successively. The second panel "Select extraction algorithm", calculations for the parameter's extractions are done with LM algorithm.

The "Test for the extraction reliability" permits the user to set the option related to the extracted parameters filtering. The test involves of three authentications: the maximum error on power (absolute and relative), the maximum NRMSE, and the value of the parameters in a user defined range. In regard, the limits on the parameters can be set in the "Model Settings" panel because they vary according to the model. Moreover, the filter can operate in four modes: first automatically (it saves only if the curve passes the test), second, semi-automatically (it asks confirmation for saving if the curve fails the test), third, manually (it asks confirmation for saving for each curve), and finally disabled (it saves all the curves).

The "Global settings" panel, allows the user to choose the main conditions of the extraction Process such as:

1."Reduction". This option reduces the number of points in the *I-V* curve to speed up the optimization. The user can select a number between 1 (that means no reduction) and (theoretically) infinite. The greater the number x chosen, the greater the reduction because the algorithm uses a point every x points. (i.e., x =2 means taken the points number 1, 3, 5, …). Moreover, the value of reduction can be calculated automatically to maintain a constant number of points of the *I-V* curve.

2."Reduction at SC", has similar operation like "Reduction" but only in the current source section, between SC and MPP points "Bound (red. at SC)". This situation limits the section where the "Reduction at SC" operates. This area of procedure is defined by two points conveyed in percentage over MPP (i.e., 0% means SC point and 100% means MPP point).

3."Reduction at OC" setting, has similar manner as "Reduction" but only in the voltage source section, between MPP and OC points.

4.“Bound (red. at OC)” option limits the section where the “Reduction at OC” operates. This procedure is defined by two points expressed in percentage over MPP (i.e., 0% means MPP point and 100% means OC point).

5.“min current Rs” and “max current Rs”. The preliminary parameter requirement must be defined properly for the convergence of the algorithm. These values are the minimum and maximum values of current used to approximate the initial condition of the R_s. These values are conveyed in percentage over the I_{sc}. Additionally, the value can be calculated automatically. In this setting, the user defines a proportion with respect to the short-circuit current, varying with the irradiance. Hence, an evaluated constant interval is obtained.

6. “Start evaluate R_{sh}” setting is the starting point to evaluate the first value of the R_{sh}.
7. “min I-V points”: minimum number of point that the I-V curve must have to expand.

The “Algorithm Settings” panel comprises the settings of maximum number of iteration and the end tolerance for each algorithm.

The “Model setting” panel comprises the bounds for the optimization and the limits for the output.

7.2 Estimation of the Initial Conditions

Initial set of parameters works as a starting point for the search of the optimal configuration. It is important that the initial values still carry some sort of physical significance, otherwise the fitting procedure could easily lead to incorrect results or require a higher computational effort to find the correct results.

In literature there are many analytical correlations and approaches that can be used to perform a rough approximation of the parameters of the single diode model. The study signifies, a sequence of analytical and numerical method that have been implemented to guarantee a good estimation of the initial parameters and simplify the accurate extraction of the five parameters with the optimization algorithms.

The initial value of the diode ideality factor is assumed to be constant and equal to 1.5, while the other four parameters are extracted with the procedure mentioned above. It requires only the coordinates of three key points of the *I-V* curves: the open circuit voltage (Voc), the short circuit current (Isc) and the voltage and current at maximum power point (Vmpp, Impp). From these points, it is possible to determine all parameters according to the series resistance (Rs). The series resistance is thus determined using a rapid and iterative algorithm that solves a nonlinear equation. Once its value is extracted, the other parameters are calculated accordingly, avoiding having to deal with too many mathematical approximations.

Taking into account the transcendental equation of the equivalent circuit, three equations can be derived for the three key points of the *I-V* curve.

- The open circuit point (Voc,0):

$$0 = I_{ph} - I_o * \left(e^{\frac{V_{OC}}{n*V_{th}*N_S}} - 1 \right) - \frac{V_{OC}}{R_{sh}} \qquad \text{Equation 22}$$

- The short circuit point (0, Isc):

$$I_{SC} = I_{ph} - I_o * \left(e^{\frac{V_{OC}}{n*V_{th}*N_S}} - 1 \right) - \frac{R_S * I_{SC}}{R_{sh}} \qquad \text{Equation 23}$$

- The maximum power point (Vmpp, Impp):

$$I_{mpp} = I_{ph} - I_o * \left(e^{\frac{V_{mpp}-R_S*I_{mpp}}{n*V_{th}*N_S}} - 1 \right) - \frac{V_{mpp} + R_S * I_{mpp}}{R_{sh}} \qquad \text{Equation 24}$$

From equation(22) is possible to obtain an explicit formulation for the photogenerated current, which can be substituted in equations 23 and 24.

$$I_{ph} = I_o * \left(e^{\frac{V_{OC}}{n*V_{th}*N_S}} - 1 \right) - \frac{V_{OC}}{R_{sh}} \qquad \text{Equation 25}$$

$$I_{SC} = I_o * \left(e^{\frac{V_{OC}}{n*V_{th}*N_S}} - e^{\frac{R_S*I_{SC}}{n*V_{th}*N_S}} \right) - \frac{V_{OC} - R_S * I_{SC}}{R_{sh}} \qquad \text{Equation 26}$$

52

$$I_{mpp} = I_o * \left(e^{\frac{V_{OC}}{n*V_{th}*N_S}} - e^{\frac{V_{mpp} - R_S * I_{mpp}}{n*V_{th}*N_S}} \right) - \frac{(V_{OC} - V)_{mpp} + R_S * I_{mpp}}{R_{sh}} \qquad \text{Equation 27}$$

To explain the equations and make easier the discussion, it is possible to introduce some variables:

$$X_{OC} = e^{\frac{V_{OC}}{n*V_{th}*N_S}} \qquad \text{Equation 28}$$

$$X_{SC} = e^{\frac{R_S * I_{SC}}{n*V_{th}*N_S}} \qquad \text{Equation 29}$$

$$X_{mpp} = e^{\frac{V_{mpp} + R_S * I_{mpp}}{n*V_{th}*N_S}} \qquad \text{Equation 30}$$

Though Xoc can be estimated at STC using the information given by the manufacturer in the datasheet, Xsc and Xmpp can be estimated only if Rs is determined. On the other hand, these variables can be used to revise equations (26) and (27) as follows

$$I_{SC} * \left(1 + \frac{R_S}{R_{sh}} \right) = I_0 (X_{OC} - X_{SC}) + \frac{V_{OC}}{R_{sh}} \qquad \text{Equation 31}$$

$$I_{mpp} * \left(1 + \frac{R_S}{R_{sh}} \right) = I_0 (X_{OC} - X_{mpp}) + \frac{V_{OC} - V_{mpp}}{R_{sh}} \qquad \text{Equation 32}$$

The values found in literature, Rs is typically in the order of a few tenths of Ohms though Rsh is in the order of a few hundred. Bearing in mind these as typical values $R\_sh \gg R\_s$, so it is likely to introduce a simplifying assumption:

$$1 + \frac{R_S}{R_{sh}} \cong 1 \qquad \text{Equation 33}$$

53

Establishing this assumption in equation (31) and (32), it can be found that:

$$I_{SC} = I_O(X_{OC} - X_{SC}) + \frac{V_{OC}}{R_{sh}}$$

<div style="text-align:right">Equation 34</div>

$$I_{mpp} = I_O(X_{OC} - X_{mpp}) + \frac{V_{OC} - V_{mpp}}{R_{sh}}$$

<div style="text-align:right">Equation 35</div>

In conclusion, from these equations it is likely to obtain an interpretation for the saturation current I_O and the shunt resistance R_{sh}:

$$I_O = \frac{V_{OC}(I_{SC} - I_{mpp}) - V_{mpp} * I_{SC}}{V_{OC}(X_{mpp} - X_{SC}) - V_{mpp}(X_{OC} - X_{sc})}$$

<div style="text-align:right">Equation 36</div>

$$\frac{1}{R_{sh}} = \frac{I_{SC}(X_{mpp} - X_{SC}) + I_{mpp}(X_{OC} - X_{sc})}{V_{OC}(X_{mpp} - X_{SC}) - V_{mpp}(X_{OC} - X_{sc})}$$

<div style="text-align:right">Equation 37</div>

The only unknowns in these equations are Xmpp and Xs, which depends on the series resistance. The short circuit current and the open circuit voltage, as well as the maximum power point voltage and current, are all estimated in the pre-processing step. Thus, the photogenerated current (25), the saturation current (36) and the shunt resistance (37) are all dependent only on the series resistance. Additionally, to fully solve the problem an additional equation is needed. This equation can be derived by the maximum power point definition.

$$\left. \frac{dP}{dV} \right|_{(V_{mpp}, I_{mpp})} = V_{mpp} * \frac{dI}{dV} + I_{mpp} = 0$$

<div style="text-align:right">Equation 38</div>

$$\frac{dI}{dV}\bigg|_{(V_{mpp}, I_{mpp})} = -\frac{I_{mpp}}{V_{mpp}}$$

<div align="right">Equation 39</div>

Taking the first derivative of the corresponding equation (39) of current with respect to voltage:

$$\frac{I_{mpp}}{V_{mpp}} = \frac{I_O}{V_{mpp}.n.N_S}\left(1 - \frac{R_S.I_{mpp}}{V_{mpp}}\right)e^{\frac{V_{mpp}+R_S*I_{mpp}}{n*V_{th}*N_S}} + \frac{1}{R_{sh}}\left(1 - \frac{R_S.I_{mpp}}{V_{mpp}}\right)$$

<div align="right">Equation 40</div>

$$\frac{I_{mpp}}{V_{mpp}} = \left(\frac{I_O.X_{mpp}}{V_{mpp}.n.N_S} + \frac{1}{R_{sh}}\right)\left(1 - \frac{R_S.I_{mpp}}{V_{mpp}}\right)$$

<div align="right">Equation 41</div>

From the two equations#. We obtained another equation that permit us to calculate the parameter Rs_calculated:

$$R_{S\_Calculated} = \frac{I_{mpp}}{V_{mpp}} - \frac{1}{\left[\frac{I_O.X_{mpp}}{V_{mpp}.n.N_S} + \frac{1}{R_{sh}}\right]}$$

<div align="right">Equation 42</div>

This equation is a strongly a nonlinear equation, and it is possible to compute the value of Rs calculated through an iterative numerical process.
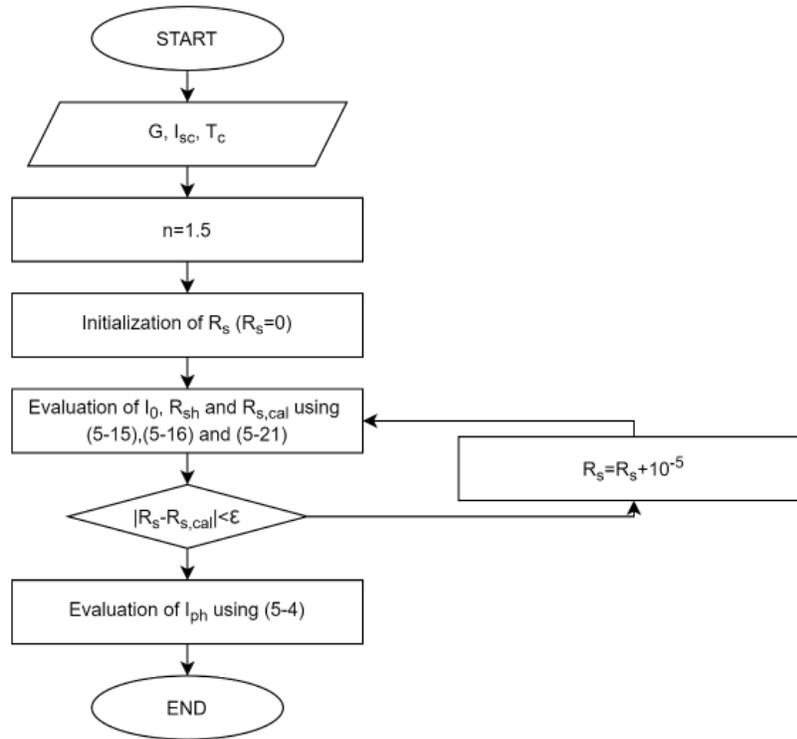
Figure 39 Flowchart of the iterative procedure used to estimate the initial conditions.

As shown in Figure 37, the series resistance is initialized considering $R_s=0$ and is gradually increased by a factor 10^{-5} at each iteration. For each value, I_0 and R_{sh} are evaluated using equations (36) and (37), as well the calculated series resistance $R_{s,calculated}$ which is compared with R_s to check the validity of the parameters found. The algorithm converges whenever the difference between R_s and $R_{s,calculated}$ is below a certain threshold.

56

Chapter 8: Stage 3-Regression

For the regression stage MATLAB scripts are written which contains all the necessary settings in the simplest manner. The settings for the parameter correlation allow to select 5 parameter model. The "Algorithm" gives the opportunity to choose dataset of the PV model to elaborate. The "Filters" gives the possibility to filter the parameters sets by irradiance and temperature.

8.1 Parameters Correlations

This part comprises in the submission of a nonlinear fitting procedure to the equations. The regression achieved are valid only for the five parameters model (i.e., I_{SC}, I_O, n, R_S, R_{sh}).

8.1.1 Photogenerated Current Correlation

The photogenerated current is proportional to the irradiance and is linear with Temperature all through, the alpha coefficient is generally given by manufacturer. The equation is expressed as following:

$$I_{ph} = I_{ph,STC} * \frac{G}{G_{STC}} * \left(1 + \alpha * \left(T_C - T_{C,STC}\right)\right)$$

Equation 43

Where:

- I_{ph} is the photogenerated current of the five parameters model (A)
- $I_{ph, STC}$ is the photogenerated current in STC (A)
- α is the short circuit temperature coefficient (K^{-1})
- G is the module irradiance (W $\cdot$ m^{-2})
- G_{STC} is the module irradiance in STC (W $\cdot$ m^{-2})
- T_C is the cell temperature (K)
- $T_{C, STC}$ is the cell temperature in STC (K)

I$_{ph, STC}$ and α are the optimization coefficients, α can be optimized or fixed to a specific value.

8.1.2. Saturation Current Correlation

The diode saturation current has a cubic proportionality with the temperature. In particular, the monocrystalline technology expresses the following equation:

$$I_O = I_{O,STC} * \left(\frac{T}{T_{STC}}\right)^3 * exp\left(\left(\frac{E_{g,STC}}{E_g} - \frac{E_g(T_C)}{T_C}\right) * \frac{1}{k_B}\right)$$

Equation 44

$$E_g = E_{g,STC} * \left(1 - 0.0002677(T_C - T_{C,STC})\right)$$

Equation 45

$$(for\ m - Si\ @\ 298\ K) \qquad E_{g,STC} = 1{,}121 \cdot q_e$$

Equation 46

- I_0 is the diode saturation current (A)
- k_B is the Boltzmann constant (J · K^{-1})
- $q_e = 1{,}602 \cdot 10^{-19}$ C is the charge of the electron
- $I_{O,\,STC}$ is the diode saturation current in STC (A)
- $E_g(T_C)$ is the energy gap at T_C (J)
- $E_{g,STC}$ is the energy gap in STC (J)

The above equation is valid only for those technology whose band gab is known such as monocrystalline silicon. some modifications are required. A new a dimensional empirical coefficient χ can be added to take in account for the different behaviors of the energy gap of other specific technologies.

$$I_O = I_{O,STC} * \left(\frac{T}{T_{STC}}\right)^3 * exp\left(\chi\left(\frac{E_{g,STC}}{E_g} - \frac{E_g(T_C)}{T_C}\right) * \frac{1}{k_B}\right)$$

Equation 47

The optimization coefficients are $I_{0,STC}$ and χ. In practice, χ can be optimized or fixed to a specific value (i.e., $\chi = 1$ to use equation).

8.1.3. Ideality Factor Correlation

The diode ideality factor is frequently deemed as constant in most applications. It has a slightly linear trend both with irradiance and temperature and can be expressed by the following formulation:

$$n = a + b * G + c * T_C \qquad \text{Equation 48}$$

Where:

• n is the diode ideality factor (-)

• a is the intercept term (-)

• b expresses the linear effect in irradiance (W^{-1} · m^2)

· c expresses the linear effect in module temperature (C^{-1})

The optimization coefficients are a, b, c.

8.1.4. Series Resistance Correlation

The series resistance has a tendency which is proportional to the temperature and logarithmical to the irradiance, according to [35]. The following equation is optimized:

$$R_S = R_{S,STC} * \frac{T_C}{T_{C,STC}} * \left(1 - \lambda_{R_s} \left(\log \frac{G}{G_{STC}} \right) \right) \qquad \text{Equation 49}$$

Where:

Academic year 2020/2021

• R_s is the series resistance (Ω)

• $R_{s,STC}$ is the series resistance at STC (Ω)

• λ_{Rs} is an empirical coefficient that expresses proportionality to the logarithmic variation of the irradiance (-)

The optimization coefficients are $R_{s,STC}$, λ_{Rs}

8.2.5. Shunt Resistance Correlation

The shunt resistance is inversely proportional with irradiance. Its expression can be written as follows:

$$R_{sh} = R_{sh,STC} * \frac{G}{G_{STC}}$$
<div align="right">Equation 50</div>

Where:

• R_{sh} is the shunt resistance (Ω)

• $R_{sh,STC}$ is the shunt resistance in STC (Ω)

The optimization coefficient is $R_{sh,STC}$.

8.2 Normalized Root Mean Square Error (NRMSE)

The Normalized Root Mean Square Error (*NRMSE*) is generally used to evaluate the errors between the experimental points and the fitting surfaces. This operation is performed for the 5 parameters of the model using the same expression. The X symbols can be replaced by the symbol of the parameter analyzed (i.e., i.e., I_{SC}, I_O, n, R_S, R_{sh}).

$$NRMSE_X = \frac{\sqrt{\dfrac{\sum_{i=1}^{N_{points}}(X_{cor} - X_{exp})^2}{N_{points}}}}{\dfrac{\sum_{i=1}^{N_{points}}(X_{exp})}{N_{points}}} * 100 \qquad \text{Equation 51}$$

Where:

• $NRMSE_X$ is the normalized root mean square error for parameter X (%)

• X_{exp} is the experimental parameter value

• X_{cor} is the estimation from correlation parameter value

• N_{points} is the number of points in the experimental samples

Chapter 9: Stage 4-Power Validation

This chapter discusses the last stage of this study which is the maximum power point and energy estimation from the weather condition (module irradiance and temperature). The goal of this work is to compare different means to estimate the energy, the power is estimated according to two different approaches. The first one is using correlations, in order to compute the measured *I-V* curve with respect to the estimated parameters. Whereas the second on is the Osterwalder method.

Equation for Power and Energy computation

The script allows to input an experimental set of data, the module datasheet information, and the correlation coefficients for the model. The power estimation is computed with the equations of the correlations described in 8.1. The five parameters (i.e. I_{SC}, I_O, n, R_S, R_{sh}) are estimated from the coefficients (i.e. $I_{ph,STC}$, α, $I_{O,STC}$, χ, a, b, c, $R_{S,STC}$, λ, $R_{sh,STC}$) are evaluated corresponding to the value of irradiance and temperature (G, T_C). Then, the parameters are used to get the *I-V* curve and the maximum power point on the curve. Afterwards, the power is determined with the Osterwald method to do the comparison. The Osterwald equation [37] is represented below:

$$P_{osterwald} = P_{STC} * \frac{G}{G_{STC}} * \left(1 + \frac{\gamma}{100} * (T_C - T_{C,STC})\right)$$

Equation 52

Where:

• $P_{Osterwald}$ is the power calculated by the Osterwald method (W)

• P_{STC} is the power in STC from the datasheet (W)

• γ is the power thermal coefficients ($\% \cdot K^{-1}$)

• G is the module irradiance ($W \cdot m^{-2}$)

• T_C is the module temperature (K)

• G_{STC} is the irradiance in STC (i.e., 1000 $W \cdot m^{-2}$)

• $T_{C, STC}$ is the module temperature in STC (i.e., 298,15 K)

The goodness of the power can be estimated with the Normalized Root Mean Square Error (NRMSE). It's the ratio between the experimental power and the estimated ones. This calculation is performed for each model using the same expression.

$$NRMSE_{P,MPP} = \frac{\sqrt{\dfrac{\sum_{i=1}^{N_{points}}(X_{MPP,model} - X_{MPP,exp})^2}{N_{points}}}}{\dfrac{\sum_{i=1}^{N_{points}}(X_{MPP,exp})}{N_{points}}} * 100 \qquad \text{Equation 53}$$

Where:

• $NRMSE_{P, MPP}$ is the normalized root mean square error on the power at MPP (%)

• $P_{MPP,exp}$ is the experimental power at MPP (W)

• $P_{MPP,model}$ is the estimated power at MPP with the model under exam (W)

• N_{points} is the number of points in the dataset (-)

The last step comprises is the energy estimation. The estimation of energy is applied by integrating with respect to time the maximum power point values. The integration is done considering a step wise function of power on which it is possible to apply the rectangular rule. This leads that for each 'step', the integral is estimated as the area of the triangle, the height of the triangle is given by the maximum power point value whereas the base by the width of the step. A step is normally counted as the time difference between each successive measurement acquisition. In this regard, the MPP point is assumed as a midpoint. Summing up, a maximum step is enforced

to avoid the integration on a large time step whenever there is a lack of measuring points close with each other.

The energy formula is calculated as:

$$E = \sum_{i=1}^{N_{tot}} P_{MPP,i} * \Delta t_i$$

Equation 54

- $P_{MPP,i}$, is the maximum power point of step i (W).
- Δt_i, is the integration time step used to compute the energy (s).

The goodness of the energy evaluation can be measured with the percentage error between the experimental energy and the estimated ones. This calculation is performed for each model using the expression

$$E_{rrE} = \frac{E_{model} - E_{exp}}{E_{exp}} * 100$$

Equation 55

Where:

• E_{rrE} is the percentage error on the energy (%)

• E_{exp} is the experimental energy (J)

• E_{model} is the estimated energy with each model (J)

Chapter 10: Analysis of Results

This chapter describes about the experimental campaign held in University of Jaen. Furthermore, it describes regarding the PV model used and its corresponding results considering all stages.

10.1 Description of Data Acquisition Campaign

The experimental campaign was conducted for four months In University of Jaen. The measuring system described in chapter 4 was used to carry out the experimental campaign. Moreover, the PV module selected for this study is the multi crystal technology were measured by the automatic tracker system. This campaign was conducted with a Kyocera KD 135GH- 2PU module.

Additionally, it is essential to state that prior to starting the experimental campaign the PV module under test was calibrated by an independent certified laboratory (CIEMAT laboratory). The objective of the calibration was to obtain the main electrical characteristics and check for the electrical response of the modules. This step was required to promise non-defective I-V curves and therefore to guarantee the accuracy and the importance of the overall study.

In this chapter a brief description of the module under-test and of the corresponding experimental campaign will be carried out, with particular emphasis on the data set available and, on the filtering, procedure applied for the purpose of this study

10.2 Description of Module

The KD 135GH- 2PU module is composed of a multi crystalline technology. Multi-crystalline cells are made by using several grains of monocrystalline silicon. In the manufacturing process, molten polycrystalline silicon is cast into ingots, which are eventually cut into very thin wafers and gathered into complete cells. Multi-crystalline cells are cheaper to produce than

monocrystalline ones because of the simpler manufacturing process required. They are, however, slightly less efficient, with average efficiencies being around 12%.

Particularly, the model under test is a Kyocera KD 135GH- 2PU module. The main specification from manufacturer and calibration are summarized in the following tables:

Source	P_{MPP} (W)	V_{OC} (V)	I_{SC} (A)	V_{MPP} (V)	I_{MPP} (A)	*FF* (%)
CIEMAT Lab	141.1	22.1	8.64	17.7	7.97	73.9%
Manufacturer	135	22.1	8.37	17.7	7.63	99.96%

Table 1 Specifications of the Kyocera KD 135GH- 2PU module.

Source	Temperature coeff P_{MPP} (W/°C)	Temperature coeff V_{OC} (V/°C)	Temperature coeff I_{SC} (A/°C)
Manufacturer	$-6.14*10^{-1}$	$-0.80*10^{-1}$	$5.01*10^{-3}$

Table 2 Temperature coefficients of the Kyocera KD 135GH- 2PU module.

The calibration of the PV module was performed in 2012. The PV module was mounted on the automatic Tracker measuring system. The corresponding experimental campaign was carried out between April and July 2021. In the four months experimental campaign a large set of data was recorded in a wide range of operating conditions. The parameters accumulated during the experimental campaign are the cell temperature and the irradiance. The range of measurements (maximum and minimum) of these parameters are reported in table:

Kyocera KD 135GH- 2PU		
Irradiance G [W/m2]	Min	Max
	400	1000
Tc [K]	Min	Max
	300	450

Table 3 Maximum and minimum ranges for irradiance and temperature.

10.3 Parameter Extraction Results

The optimization algorithms may find various sets of parameters. The objective of the parameter's extraction procedure is to achieve a set of parameters that can estimate as best as possible the I-V curves. Nonphysical solutions, to be discarded, are present in this set of parameters. This process has been applied to all the 196 curves. Nevertheless, after the extraction, the set of parameters has been filtered to remove those affected by overfitting. The following filters have been applied:

- NRMSE below 0.02
- Error on Maximum Power below 1%.
- Series Resistance below 1 Ω.
- Shunt Resistance below 2000 Ω.

In the end, the feasible parameters left were 195 for Levenberg-Marquardt algorithm.

10.4 Parameter Correlations Results

The extracted parameters are used to approximate the correlations with respect to the irradiance and cell temperature. The correlations used are those presented in chapter 6. The trend of each parameter is graphically presented for the LM optimization. Now, the term "experimental" in the legends shows the points obtained after using the LM methods. Likewise, the term "correlation" denotes the points out the trend that show the found correlation. The parameters are represented in the following order:

1. photogenerated current
2. diode saturation current,
3. diode ideality factor
4. series resistance
5. shunt resistance.

The photogenerated current (I_{ph}) introduces a main dependence on the irradiance as shown in Figure 38.

It can be noticed that the dependency on cell temperature is negligible. Moreover, the correlation equation is derived from the equation (43). The $I_{ph,STC}$ coefficient is optimized by the correlation whilst the α is taken from the manufacturer datasheet.
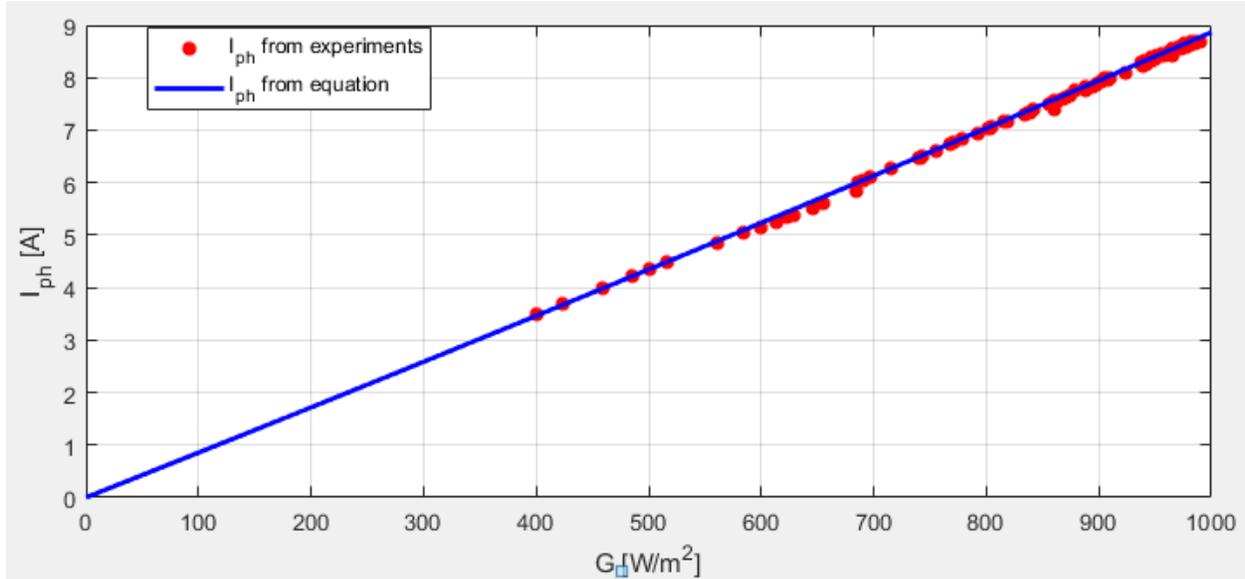
Figure 40 $I_{ph.}$ tendency with irradiance using LM algorithm.

$$I_{ph} = 8.64 * \frac{G}{G_{STC}} * \left(1 + \alpha * \left(T_C - T_{C,STC}\right)\right)$$

Equation 56

The orange dots represent the I_{ph} values from the LM optimization (i.e., experimental) whereas the blue line shows the trend of the correlation in equation 56. The goodness of the correlation is verified by the NRMSE value of 0.36%.

The diode saturation current (I_0) shows only dependency on the cell temperature. The correlation equation comes from the equation (44). The $I_{O, STC}$ coefficient were optimized by the correlation. Figure 39 noticeably show the tendency.
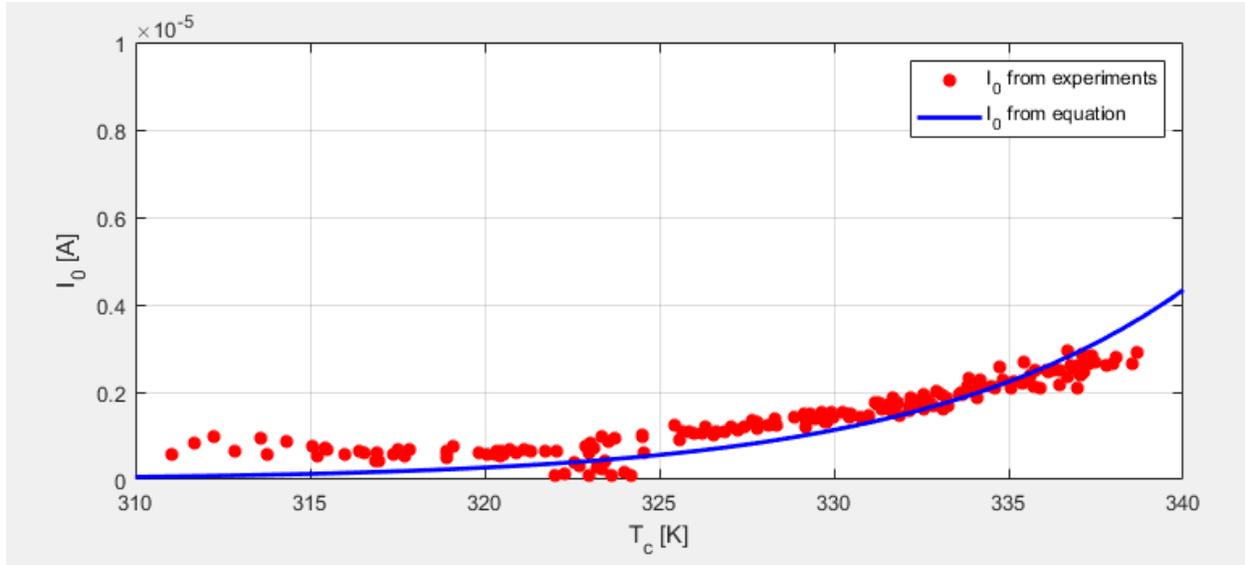
Figure 41 I_O tendency with temperature using LM algorithm.

$$I_O = 8.90 * 10^{-9} * \left(\frac{T}{T_{STC}}\right)^3 * exp\left(\left(\frac{E_{g,STC}}{E_g} - \frac{E_g(T_C)}{T_C}\right) * \frac{1}{k_B}\right) \qquad \text{Equation 57}$$

The orange dots denote the I_0 values from the LM optimization (i.e., experimental) while the blue line displays the curve of the correlation in equation 57. The goodness of the correlation is verified by the *NRMSE* value of 26.31%. Furthermore, this value is typical for the diode saturation current correlation.

The diode ideality factor (n) generates low difference with irradiance and cell temperature. The correlation equation is obtained from the equation (48). Moreover, the coefficients a, b and c are optimized by the correlation. Figure 40 clearly exhibit the irradiance and temperature tendency for LM methods.
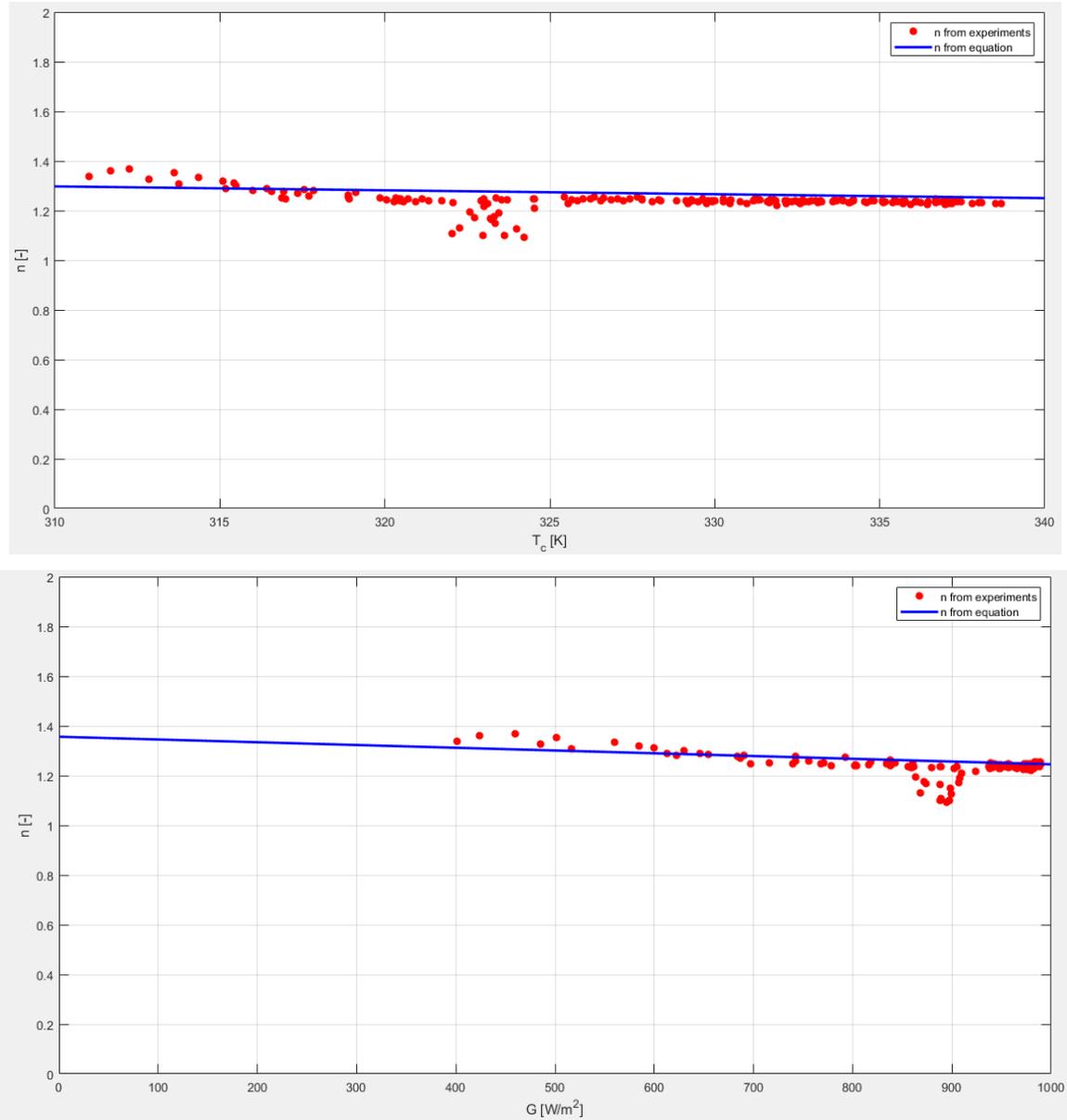
Figure 42 n tendency with irradiance and temperature using LM algorithm.

$$n = 0.718 + (-0.000258) * G + 0.0021 * T_C \qquad \text{Equation 58}$$

The red dots represent the n values from the LM optimization (i.e., experimental) whereas the blue line displays the trend of the correlation in equation 58. The goodness of the correlation is validated by the *NRMSE* value of 2.41%. Lastly, this value is typical for the diode ideality factor correlation. The ideality factor shows an increased tendency with both irradiance and temperature.

70

The series resistance (R_S) shows variation with irradiance and cell temperature. The correlation equation comes from the equation (49). The R_S, STC and λ_{Rs} coefficients are optimized by the correlation. Figure 41 evidently report the irradiance and temperature tendencies respectively for LM methods.
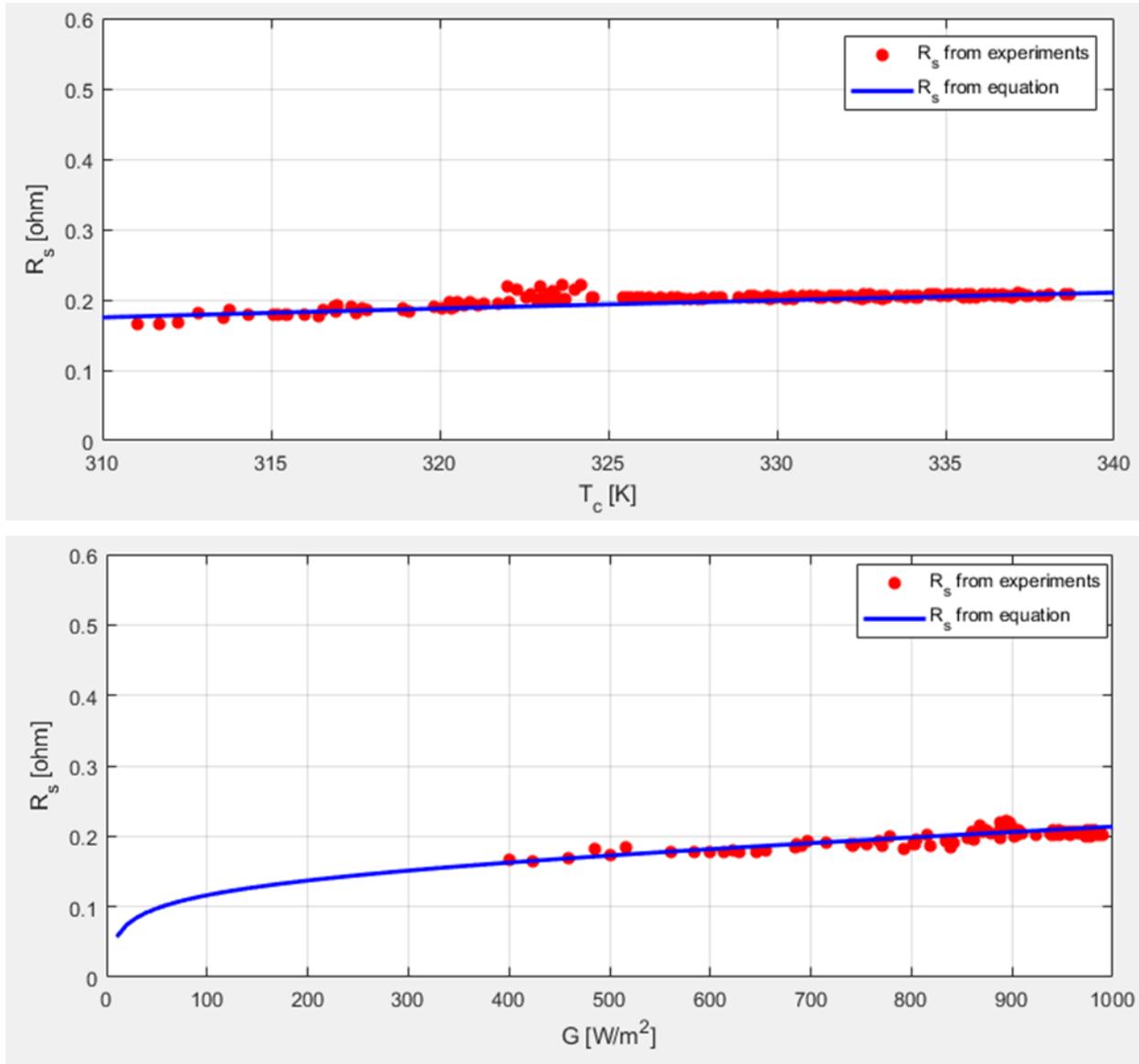
Figure 43 Rs tendency with irradiance and temperature using LM algorithm.

71

$$R_s = 0.186 * \frac{T_C}{T_{C,STC}} * \left(1 - (-0.145)\left(\log\frac{G}{G_{STC}}\right)\right)$$

Equation 59

The orange dots display the R_S values from the LM optimization (i.e., experimental) whereas the blue line displays the curve of the correlation in equation (59). The goodness of the correlation is verified by the NRMSE value of 2.51%. This value is typical for the series resistance correlation. The series resistance demonstrates an increased tendency with both irradiance and temperature.

The shunt resistance (R_{sh}) displays the variation with irradiance and cell temperature. The correlation equation comes from the equation (50) (43). The $R_{sh,STC}$ coefficient is optimized by the correlation. Figure 42 demonstrate the irradiance tendency respectively for LM methods.
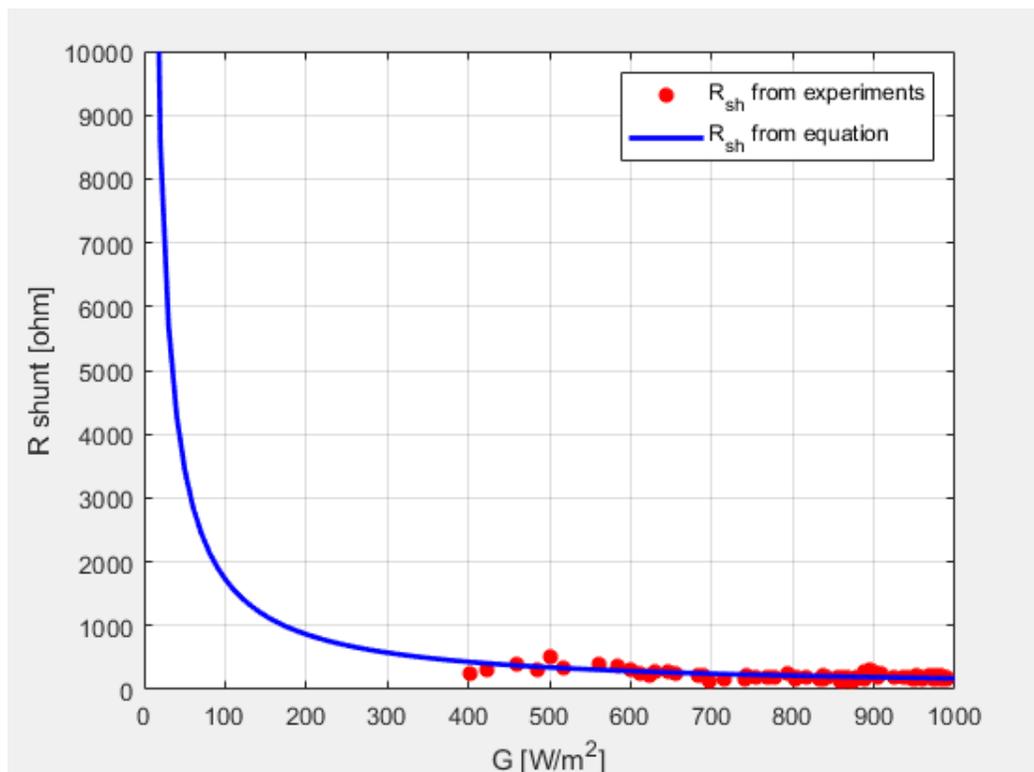
Figure 44 R_{sh} tendency with irradiance using LM algorithm.

72

$$R_{sh} = 173 * \frac{G}{G_{STC}}$$ Equation 60

The red dots represent the R_{sh} values from the LM optimization (i.e., experimental) whereas the blue line indicates the trend of the correlation in equation (60). The plot demonstrates the tendency of the shunt resistance, and the goodness of the correlation is verified by the NRMSE value of 18.31%.

The list correlation coefficients are reported in Table

Correlation coefficients	Levenberg-Marquardt (LM) method
$I_{ph,STC}$ (A)	8.64
$I_{O,STC}$ (A)	$8.90*10^{-9}$
a (-)	0.781
b ($W^{-2} \cdot m^2$)	-0.000258
c (C^{-1})	0.00210
$R_{S,STC}$ (Ω)	0.186
λ_{Rs} (-)	-0.145
$R_{sh,STC}$ (Ω)	173

Table 4 Correlation coefficients for the Kyocera KD 135GH- 2PU module.

Lastly the analysis on the results of the correlation includes in redrawing the experimental *I-V* curve with the found correlations. Figure 45 shows the seven experimental *I-V* curves with the respective approximations found with the correlations.
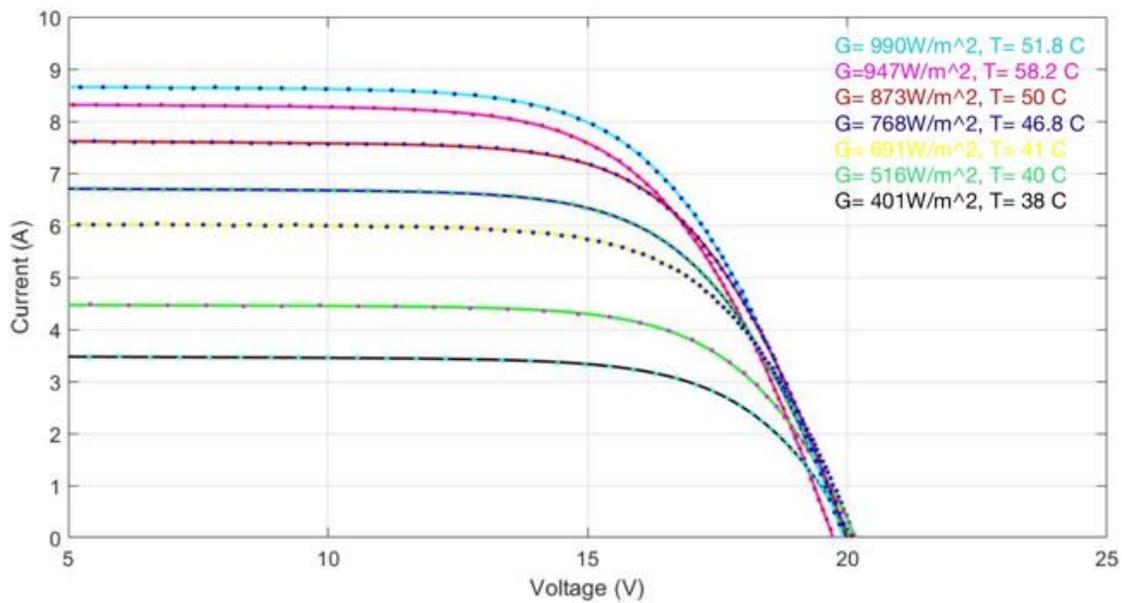
Figure 45 I-V curves experimentally measured (dots) and trend estimated with the LM method.

10.5 Power Validation and Energy Computation Results

The maximum power experimental data are compared to the maximum power estimated data from the two models (i.e., LM, and Osterwald). This comparison can be representing the Figure 46 that shows the shape of the power during a day. In particular, the LM method presents a *NRMSE* value of 4.98% for that day. On the other hand, the Osterwald method overestimates even more the experimental data. In this case, the *NRMSE* value is 9.69%.). In summary, the use of the proposed correlation method leads to a reduction of the NRMSE, compared to the Osterwald method.
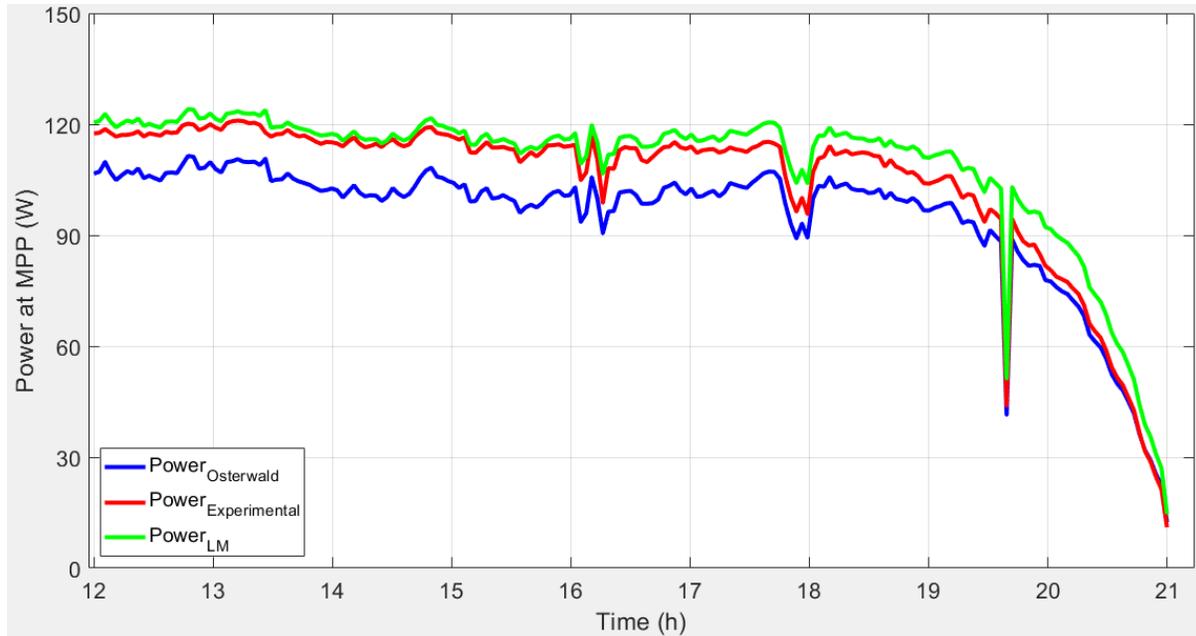
Figure 46 Comparison of power estimation for a sunny day.

A set of 195 curves of data is obtained with the LM algorithm, while the largest error on the MPP with LM dataset coincide with error on energy.

Chapter 11: Conclusions

The operation of Photovoltaic (PV) generators can be expressed by an equivalent circuit with a variable number of parameters, which are, normally, assumed to be constant. Though, the knowledge of their dependence with respect to irradiance and cell temperature permits to foresee the produced power of photovoltaic arrays in any weather condition. The experimental work for this work is done in Universidad de Jaén, Spain.

For this thesis a Graphical User interface (GUI) is developed in MATLAB to allow the wide analysis of a huge dataset of experimental data. Specifically, the tool permits to execute four operations: the preprocessing of the dataset; the extraction of the circuit parameters; the identification of equations, aiming at describing the dependence of each parameter with respect to irradiance and cell temperature, and the comparison between experimental energy can be predicted by various methods.

The GUI is used for a multi crystalline silicon module of Kyocera KD 135GH- 2PU with rated power of 135W. For this module,196 I-V curves are chosen for the parameter's extraction. The eliminated data are omitted due to different reasons such as the measurement errors and the mismatch conditions. The photovoltaic module performance is shown by the single diode model, with an equivalent circuit comprising of five parameters. After that, the extraction procedure is performed using the Levenberg-Marquardt (LM) optimization method.

Furthermore, two additional filters are applied to the results of the parameters extraction in order to exclude the parameters set leading to a high error in the Maximum Power Point (MPP). A set of 195 curves is obtained with the LM algorithm, while the largest error on the MPP with LM dataset coincide with error on energy. Starting from these datasets, the equations illustrating the dependence of each parameter with respect to irradiance and cell temperature are identified. The correlations show comparable results to the examined datasets. Concerning the necessary parameters, the photogenerated current and the series resistance present, respectively, a Normalized Root Mean Square Error (NRMSE) of 0.36% and 2.51% for both the datasets, while the NRMSE of the reverse saturation current ranges between 26.31% (LM). Lastly is a comparison

between the experimental energy and the predicted value with optimized equations is performed. Furthermore, the proposed correlations are compared to the Osterwalder Model (OM), which is the easiest and most common theoretical model used in literature to predict PV production. The results show that the LM equations predict PV energy with the lowest error, providing a deviation from experimental data of 4.98%, while the OM results exhibit, respectively, an error of 9.69%. In summary, the use of the proposed correlation method leads to a reduction of the NRMSE, compared to the Osterwald method.

12. Bibliography

[1]   B. Anco S, Photovoltaics for Commercial and Utilities Power Generation, Lilburn (GA, USA): Fairmont Press, Inc., 2012.

[2]   F. Spertino, Lezioni di "Solar Photovoltaic System', Torino: Politecnico di Torino, 2019/2020.

[3]   M. Alonso Abella, Sistemas fotovoltaicos: introducción al diseño y dimensionado de instalaciones solares fotovoltaicas, Madrid: SAPT Publicaciones Técnicas S.L., 2005.

[4]   D. Murgia, «Tecniche per l'identificazione dei difetti e per l'analisi delle performance nei moduli fotovoltaici,» Politecnico di Torino, Tesi di Laurea Magistrale, 2018.

[5]   A. Scaiola, «Innovative technique to estimate the performance of a photovoltaic generator using the parameters of the single diode model equivalent circuit, » Politecnico di Torino, Tesi di Laurea Magistrale, 2019.

[6]   [Online]. Available: https://www.futurasun.com/wp-content/uploads/2018/ 04/pannello-monocristallino_dettaglio.jpg.

[7]   National Renewable Energy Laboratory (NREL), «Champion Photovoltaic Module Efficiency Chart,» NREL, 2019.

[8]   [Online].   Available: http://www.fotovoltaicosulweb.it/immagini/upload/ guida/policristalline_panels1.jpg.

[9]   SANYO Component Europe GmbH Solar Division, «HIT-240HDE4 HIT- 235HDE4 datasheet, » SANYO Component Europe GmbH, 2009.

[10]   [Online]. Available: https://www.vpsolar.com/wp-content/uploads/2018/04/ tecnologia-perc-funzionamento.jpg.

[11]   [Online]. Available: https://zeroemission.eu/wp-content/uploads/2020/02/ Thin-film-Solar-Cell-425x405.jpg.

[12]   [Online].   Available: https://opentextbc.ca/chemistry/wp-content/uploads/sites/150/2016/05/CNX_Chem_08_04_Band.jpg.

[13]   [Online]. Available: https://solarconsultant.ca/wp-content/uploads/ 2017/05/Silicon-Solar-Cell-Construction.png.

[14]   U. Gangopadhyay, S. Das and S. Jana, "State of the Art of Photovoltaic Technology," in International Conference on Solar Energy Photovoltaics, Bhubaneswar, India, 2013.

[14]   National Renewable Energy Laboratory (NREL), "Best Research-Cell Efficiency Chart," NREL, 2020.

[15]   S. Mishra e D. Sharma, «Control of photovoltaic technology, » in *Electric Renewable Energy Systems*, Elsevier, 2016, pp. 457-486.

[16]   A. Haque, «Solar energy, » in *Electric Renewable Energy Systems*, Elsevier, 2016, pp. 40-59.

[17]   [Online].   Available: https://www.etechnog.com/2019/05/diode-used-solarpanel-relay.html.

[18]   [Online]. Available: https://jerseyfirstis.com/wp-content/uploads/2018/ 06/solar-panel-inspection.jpg

[19]   S. Gulkowski, J. V. Munoz Diez, J. Aguilera Tejero and G. Nofuentes, "Energy," Energy, vol. 172, pp. 380-390, 2019.

[20]   D. W. Marquardt, «An Algorithm for Least-Squares Estimation of Nonlinear Parameters, » *Journal of the Society for Industrial and Applied Mathematics,* vol. 11, n. 2, pp. 431-441, 1963.

[21]   J. A. Nelder e R. Mead, «A simple method for function minimization, » *The Computer Journal,* vol. 7, n. 4, pp. 308-313, 1965.

[22]   G. Chicco, «Note sull'analisi e sull'ottimizzazione dei sistemi elettrici di distribuzione,» Politecnico di Torino, 2004.

[23]   G. Blaesser and D. Munro, "Guidelines for the Assessment of Photovoltaic Plants, Document C, Initial and Periodic Tests on PV Plants," Office for Official Publications of the European Communities, Ispra, Italia, 1995.

[24]   E. Durán, M. Piliougine, M. Sidrach-de-Cardona, J. Galán e J. Andújar, «Different methods to obtain the I–V curve of PV modules: A review,» in *2008 33rd IEEE Photovoltaic Specialists Conference*, San Diego, CA, USA, 2008.

[25]   F. Spertino, J. Ahmad, A. Ciocia, P. Di Leo, A. F. Murtaza e M. Chiaberge, «Capacitor charging method for I–V curve tracer and MPPT in photovoltaic systems,» *Solar Energy,* vol. 119, pp. 461-473, 2015.

[26]   R. Núñez, C. Domínguez, S. Askins, M. Victoria, R. Herrero, I. Antón e G. Sala, «Determination of spectral variations by means of component cells useful for CPV rating and design,» *Progress in Photovoltaics,* vol. 24, n. 5, pp. 663-679, May 2016.

[27]   B. García Domingo, «Análisis, caracterización y modelado del comportamiento en exterior de módulos de concentración fotovoltaica,» Universidad de Jaén, Tesis Doctoral, 2014.

[28]   Z. Stokes e A. Kaknevicius, «Reverse Current Protection in Load Switches, » TexasInstruments Inc., May 2016.

[29]   S. Gulkowski, J. V. Muñoz Diez, J. Aguilera Tejero e G. Nofuentes, «Computational modeling and experimental analysis of heterojunction with intrinsic thin-layer photovoltaic module under different environmental conditions, » *Energy,* vol. 172, pp. 380-390, 2019.

[30]   F. Spertino, A. Ciocia, P. Di Leo, S. Fichera, G. Malgaroli e . A. Ratclif, «Toward the Complete Self-Sufficiency of an nZEBs Microgrid by Photovoltaic Generators and Heat Pumps: Methods and Applications, » *IEEE Transactions On Industry Applications,* vol. 55, n. 6, pp. 7028-7040, Nov.-Dec. 2019..

[31]   M. Norton, A. M. Gracia Amillo e R. Galleano, «Comparison of solar spectral irradiance 2015

[32]   F. Ghani, M. Duke e J. Carson, «Numerical calculation of series and shunt resistance of a photovoltaic cell using the Lambert W-function: Experimental evaluation, » *Solar Energy,* vol. 87, pp. 246-253, January 2013.

[33]   A. Molina-Garcia, M. Bueso, M. Kessler, J. Guerrero-Perez, J. Fuentes and E. Gomez-Lazaro, "CdTe thin-film solar module modeling using a non-linear regression approach," in 17th Power system computation Conference, Stockholm (Sweden), 2011.

[34]   R. Majdoul, E. Abdelmounim, M. Aboulfatah, A. w. Touati, A. Moutabir e A. Abouloifa, «Combined analytical and numerical approach to determine the four parameters of the photovoltaic cells models, » in *2015 International Conference on Electrical and Information Technologies (ICEIT)*, Marrakech, 2015.

[35]   A. K. Tossa, Y. Soro, Y. Azoumah e D. Yamegueu, «A new approach to estimate the performance and energy productivity of photovoltaic modules in real operating conditions, » *Solar Energy,* vol. 110, pp. 543-560, 2014.

[36]   M. Wolf e H. Rauschenbach, «Series resistance effects on solar cell measurements, » *Advanced Energy Conversion,* vol. 3, n. 2, pp. 455-479, 1963.

[37]   C. R. Osterwald, «Translation of device performance measurements to reference conditions, » *Solar Cells,* vol. 18, n. 3-4, pp. 269-279, September–October 1985.

13. Appendix

Annex A: Technical datasheet of measurement equipment

A.1 Technical datasheet Agilent 34411A Multimeters

Measurement Characteristics

DC Voltage

Measurement Method:
Continuously integrating multi-slope IV A/D converter

Linearity: 0.0002% of reading
(10 V range) + 0.0001% of range

Input Resistance:
0.1 V, 1 V, 10 V 10 MΩ or > 10 GΩ
Ranges (Selectable)
100 V, 1000 V 10 MΩ ± 1%
Ranges (Fixed)

Input Bias Current: < 50 pA at 25 °C

Input Protection: 1000 V

DC CMRR: 140 dB[1]

True RMS AC Voltage

Measurement Method:
AC-coupled True RMS measurement. Digital sampling with anti-alias filter.

Crest Factor:
No additional error for crest factors < 10. Limited by peak input and 300 kHz bandwidth.

Peak Input:
300% of range or 1100 V

Overload Ranging:
Will select higher range if peak input overload is detected during auto range. Overload is reported in manual ranging.

AC CMR: 70 dB[2]

Maximum Input: 400 Vdc, 1100 Vpk

Input Impedance:
1 MΩ ± 2% in parallel with < 150 pF

Input Protection: 750 V_{rms} all ranges

Resistance

Measurement Method:
Selectable 2-wire or 4-wire. Current source referenced to LO input.

Offset Compensation:
Selectable on the 100 Ω, 1 kΩ, and 10 kΩ ranges

Max. Lead Resistance (4-wire):
10% of range per lead for 100 Ω, 1 kΩ. 1 kΩ per lead on all other ranges

Input Protection:
1000 V on all ranges

DC Current

Current Shunt:
200 Ω for 100 μA, 1 mA
2 Ω for 10 mA, 100 mA
0.1 Ω for 1 A, 3 A

Input Protection: 3 A, 250 V fuse

True RMS AC Current

Measurement Method:
AC-coupled True RMS measurement. Directly coupled to the fuse and shunt. Digital sampling with anti-alias filter.

Current Shunt:
200 Ω for 100 μA, 1 mA
2 Ω for 10 mA, 100 mA
0.1 Ω for 1 A, 3 A

Maximum Input:
The peak value of the DC + AC current must be < 300% of range. The RMS current must be < 3 A including the DC current content.

Input Protection: 3 A, 250 V fuse

Frequency and Period

Measurement Method:
Reciprocal-counting technique. AC-coupled input using the AC voltage measurement function.

Input Impedance:
1 MΩ ± 2% in parallel with < 150 pF

Input Protection: 750 V_{rms} all ranges

Capacitance

Measurement Method:
Current input with measurement of resulting ramp.

Connection Type: 2-wire

Temperature

Thermistor:
2.2 kΩ, 5 kΩ, and 10 kΩ

RTD: α = 0.00385
R_o from 49 Ω to 2.1 kΩ

Continuity/Diode Test

Response Time:
300 samples/sec with audible tone

Continuity Threshold: Fixed at 10 Ω

Operating Characteristics
Maximum readings/second

Function[3]	Digits 4.5	5.5	6.5
DCV	50 k[4]	10 k	1 k
2-wire Ω	50 k[4]	10 k	1 k
DCI	50 k[4]	10 k	1 k
Frequency	500	90	10
Period	500	90	10
Filter setting	fast	med	slow
ACV	500	150	50
ACI	500	150	50

1. For 1 kΩ unbalanced in LO lead, ± 500 V peak maximum
2. For 1 kΩ unbalanced in LO lead and < 60 Hz, ± 500 V peak maximum
3. Maximum rate for DCV, DCI, and resistance functions (using zero settling delay, autozero off, manual range)
4. 34411A only

Additional 34411A Specifications

Resolution: See table on page 4

Overall Bandwidth, DCV & DCI:
15 kHz typical @ 20 μs aperture (–3 dB)

Triggering: Pre/Post, Int/Ext, Pos/Neg

Timebase Resolution: 19.9524 μs 0.01% accuracy

Trigger Jitter:
2 μs (p–p), 20 μs (p–p) when pre-triggered

Spurious-Free Dynamic Range & Signal to Noise Distortion Ratio

Function DCV	Range	Spur-Free	SNDR
	1 V	–75 dB	60 dB
	10 V[1]	–70 dB	60 dB
	100 V	–75 dB	60 dB

[1] 10 V range: 2 V (p–p) < signal < 16 V (p–p)

Triggering and Memory

Reading Hold Sensitivity: 1% of reading

Samples per Trigger:
1 to 50,000 (34410A)
1 to 1,000,000 (34411A)

Trigger Delay: 0 to 3600 s (20 μs step size)

External Trigger:
Programmable edge, Low-power TTL compatible
Delay: < 1 μs **Max rate:** 5,000/s
Jitter: < 1 μs **Min Pulsewidth:** 1 μs

Voltmeter Complete: 3 V Logic output, 2 μs pulse with programmable edge

Nonvolatile Memory: 50,000 readings

Volatile Memory:
50,000 readings (34410A)
1,000,000 readings (34411A)

Sample Timer:
Range: 0 to 3600 s (20 μs step sizes)
Jitter: < 100 ns

General Specifications

Power Supply:
100 V/120 V/220 V/240 V ± 10%

Power Line Frequency:
45 Hz to 66 Hz and 360 Hz to 440 Hz, Automatically sensed at power-on

Power Consumption: 25 VA peak (16 W average)

Operating Environment: Full accuracy for 0 °C to 55 °C, 80% R.H. at 40 °C non-condensing

Storage Temperature: –40 °C to 70 °C

Weight: 3.72 kg (8.2 lbs)

Safety: IEC 61010-1, EN 61010-1, UL 61010-1, CAN/CSA-C22.2 No. 61010-1, Refer to Declarations of Conformity for current revisions. Measurement CAT II 300 V, CAT I 1000 V. Pollution Degree 2

EMC: IEC 61326, EN 61326, CISPR 11, ICES-001, AS/NZS 2064.1, Refer to Declaration of Conformity for current revisions.

Vibration & Shock: MIL-T-28800E, Type III, Class 5 (Sine Only)

LXI Compliance: LXI Class C, ver. 1.0

Warranty: 3 year standard

A-to-D Converter Noise Performance

Integration Time (NPLC)	Resolution (ppm of range)[1]	Normal Mode Rejection (dB)[2]	Readings/Second[4]
0.001[5]	30	0	50,000
0.002[5]	15	0	25,000
0.006	6	0	10,000
0.02	3	0	3,000
0.06	1.5	0	1,000
0.2	0.7	0	300
1	0.3	55	60 (50)
2	0.2	110[3]	30 (25)
10	0.1	110[3]	6 (5)
100	0.03	110[3]	0.6 (0.5)

1. Resolution is defined as the typical DCV 10 V range RMS noise. Auto-zero on for NPLC ≥ 1. See manual for additional noise characteristics.
2. Normal mode rejection for power line frequency ± 0.1%.
3. For power-line frequency ± 1% 75 dB and for ± 3% 55 dB.
4. Maximum rate with auto-zero off for 60 Hz and (50 Hz) operation.
5. Only available for the 34411A.
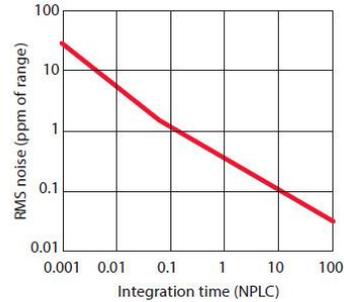
System Reading and Throughput Rates

DMM memory to PC (Maximum reading rate out of memory[6]
Drawing – Path B

Reading Format	GPIB Readings/s	USB 2.0 Readings/s	LAN (VXI-11) Readings/s	LAN (Sockets) Readings/s
ASCII	4,000	8,500	7,000	8,500
32-bit Binary	89,000	265,000	110,000	270,000
64-bit Binary	47,000	154,000	60,000	160,000

System Reading Architecture
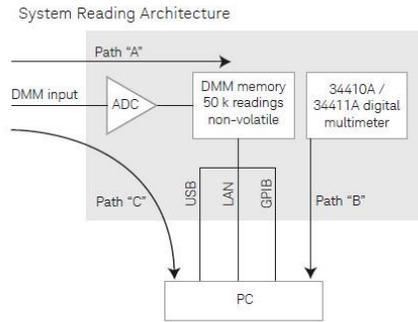
Direct I/O Measurements (Single reading – measure and I/O time)[6]

Drawing - Path C

Function	Resolution (NPLC)	GPIB ms	USB 2.0 ms	LAN (VXI-11) ms	LAN (sockets) ms	Maximum Reading Rate into Memory or to Direct I/O (Readings/s) Drawing – Path A or C
DCV/2-wire Resistance	0.006 (0.001)	2.6	2.9	4.6	3.2	10,000 (50,000)
ACV/ Frequency	Fast Filter 1 ms gate	10.0	10.0	10.0	10.0	500

6. 1/2 scale input signal, immediate trigger, trigger delay 0, auto-zero off, auto-range off, no math, null off, 60 Hz line frequency. Specifications are for 34410A or (34411A). See manual for performance on other functions.

System Performance

	Function Change (ms)[7]	Range Change (ms)[8] LAN/GPIB	Auto-range (ms)[9]	Maximum External Trigger Rate	Maximum Internal Trigger Rate[10]
DCV/2-wire Resistance	22	3.9/2.6	7.5	5,000/s	10,000/s (50,000/s)
ACV/ Frequency	37	6.5/6.4	19	500/s	500/s

7. Time to change from 2-wire Resistance to this specified function, or DCV to 2-wire Resistance using the SCPI "FUNC" command.
8. Time to change from one range to the next higher range, ≤ 10 V, ≤ 10 MΩ.
9. Time to automatically change one range and be ready for the new measurement, ≤ 10 V, ≤ 10 MΩ.
10. Specifications are for 34410A or (34411A).

Academic year 2020/2021

Accuracy Specifications ± (% of reading + % of range)[1]

Function	Range[3]	Frequency, Test Current or Burden Voltage	24 Hour[2] Tcal ± 1 °C	90 Day Tcal ± 5 °C	1 Year Tcal ± 5 °C	Temperature Coefficient/°C 0 °C to (Tcal -5 °C) (Tcal +5 °C) to 55 °C
DC Voltage	100.0000 mV		0.0030 + 0.0030	0.0040 + 0.0035	0.0050 + 0.0035	0.0005 + 0.0005
	1.000000 V		0.0020 + 0.0006	0.0030 + 0.0007	0.0035 + 0.0007	0.0005 + 0.0001
	10.00000 V		**0.0015 + 0.0004**	**0.0020 + 0.0005**	**0.0030 + 0.0005**	**0.0005 + 0.0001**
	100.0000 V		0.0020 + 0.0006	0.0035 + 0.0006	0.0040 + 0.0006	0.0005 + 0.0001
	1000.000 V[4]		0.0020 + 0.0006	0.0035 + 0.0006	0.0040 + 0.0006	0.0005 + 0.0001
True RMS AC Voltage[5]	100.0000 mV to 750.000 V	3 Hz – 5 Hz	0.50 + 0.02	0.50 + 0.03	0.50 + 0.03	0.010 + 0.003
		5 Hz – 10 Hz	0.10 + 0.02	0.10 + 0.03	0.10 + 0.03	0.008 + 0.003
		10 Hz – 20 kHz	**0.02 + 0.02**	**0.05 + 0.03**	**0.06 + 0.03**	**0.005 + 0.003**
		20 kHz – 50 kHz	0.05 + 0.04	0.09 + 0.05	0.10 + 0.05	0.010 + 0.005
		50 kHz – 100 kHz	0.20 + 0.08	0.30 + 0.08	0.40 + 0.08	0.020 + 0.008
		100 kHz – 300 kHz	1.00 + 0.50	1.20 + 0.50	1.20 + 0.50	0.120 + 0.020
Resistance[6]	100.0000 Ω	1 mA	0.0030 + 0.0030	0.008 + 0.004	0.010 + 0.004	0.0006 + 0.0005
	1.000000 kΩ	1 mA	0.0020 + 0.0005	0.007 + 0.001	0.010 + 0.001	0.0006 + 0.0001
	10.00000 kΩ	**100 µA**	**0.0020 + 0.0005**	**0.007 + 0.001**	**0.010 + 0.001**	**0.0006 + 0.0001**
	100.0000 kΩ	10 µA	0.0020 + 0.0005	0.007 + 0.001	0.010 + 0.001	0.0006 + 0.0001
	1.000000 MΩ	5 µA	0.0020 + 0.0010	0.010 + 0.001	0.012 + 0.001	0.0010 + 0.0002
	10.00000 MΩ	500 nA	0.0100 + 0.0010	0.030 + 0.001	0.040 + 0.001	0.0030 + 0.0004
	100.0000 MΩ	500 nA ∥ 10 MΩ	0.200 + 0.001	0.600 + 0.001	0.800 + 0.001	0.1000 + 0.0001
	1.000000 GΩ	500 nA ∥ 10 MΩ	2.000 + 0.001	6.000 + 0.001	8.000 + 0.001	1.0000 + 0.0001
DC Current	100.0000 µA	< 0.03V	0.010 + 0.020	0.040 + 0.025	0.050 + 0.025	0.0020 + 0.0030
	1.000000 mA	**< 0.3 V**	**0.007 + 0.006**	**0.030 + 0.006**	**0.050 + 0.006**	**0.0020 + 0.0005**
	10.00000 mA	< 0.03V	0.007 + 0.020	0.030 + 0.020	0.050 + 0.020	0.0020 + 0.0020
	100.0000 mA	< 0.3 V	0.010 + 0.004	0.030 + 0.005	0.050 + 0.005	0.0020 + 0.0005
	1.000000 A	< 0.8 V	0.050 + 0.006	0.080 + 0.010	0.100 + 0.010	0.0050 + 0.0010
	3.000000 A	< 2.0 V	0.100 + 0.020	0.120 + 0.020	0.150 + 0.020	0.0050 + 0.0020
True RMS AC Current[7]	100.0000 µA to 3.00000 A	**3 Hz – 5 kHz**	**0.10 + 0.04**	**0.10 + 0.04**	**0.10 + 0.04**	**0.015 + 0.006**
		5 kHz – 10 kHz	0.20 + 0.04	0.20 + 0.04	0.20 + 0.04	0.030 + 0.006
Frequency or Period	100 mV to 750 V	3 Hz – 5 Hz	0.070 + 0.000	0.070 + 0.000	0.070 + 0.000	0.005 + 0.000
		5 Hz – 10 Hz	0.040 + 0.000	0.040 + 0.000	0.040 + 0.000	0.005 + 0.000
		10 Hz – 40 Hz	0.020 + 0.000	0.020 + 0.000	0.020 + 0.000	0.001 + 0.000
		40 Hz – 300 kHz	**0.005 + 0.000**	**0.006 + 0.000**	**0.007 + 0.000**	**0.001 + 0.000**
Capacitance[8]	1.0000 nF	500 nA	0.50 + 0.50	0.50 + 0.50	0.50 + 0.50	0.05 + 0.05
	10.000 nF	1 µA	0.40 + 0.10	0.40 + 0.10	0.40 + 0.10	0.05 + 0.01
	100.00 nF	10 µA	0.40 + 0.10	0.40 + 0.10	0.40 + 0.10	0.01 + 0.01
	1.0000 µF	10 µA	0.40 + 0.10	0.40 + 0.10	0.40 + 0.10	0.01 + 0.01
	10.000 µF	100 µA	0.40 + 0.10	0.40 + 0.10	0.40 + 0.10	0.01 + 0.01
Temperature[9]						
RTD	-200 °C to 600 °C		0.06 °C	0.06 °C	0.06 °C	0.003 °C
Thermistor	-80 °C to 150 °C		0.08 °C	0.08 °C	0.08 °C	0.002 °C
Continuity	1000.0 Ω	1 mA	0.002 + 0.010	0.008 + 0.020	0.010 + 0.020	0.0010 + 0.0020
Diode Test[10]	1.0000 V	1 mA	0.002 + 0.010	0.008 + 0.020	0.010 + 0.020	0.0010 + 0.0020

1. Specifications are for 90 minute warm-up and 100 PLC.
2. Relative to calibration standards.
3. 20% overrange on all ranges, except DCV 1000 V, ACV 750 V, DCI and ACI 3 A ranges.
4. For each additional volt over ± 500 V add 0.02 mV of error.
5. Specifications are for sinewave input > 0.3% of range and > 1 mVrms. Add 30 µV error for frequencies below 1 kHz. 750 VAC range limited to 8 x 107 Volts-Hz. For each additional volt over 300 Vrms add 0.7 mVrms of error.
6. Specifications are for 4-wire resistance measurements, or 2-wire using Math Null. Without Math Null, add 0.2 Ω additional error in 2-wire resistance measurements.
7. Specifications are for sinewave input > 1% of range and > 10 µArms. Frequencies > 5 kHz are typical for all ranges. For the 3 A range (all frequencies) add 0.05% of reading + 0.02% of range to listed specifications.
8. Specifications are for 1-hour warm-up using Math Null. Additional errors may occur for non-film capacitors.
9. For total measurement accuracy, add temperature probe error.
10. Accuracy specifications are for the voltage measured at the input terminals only. 1 mA test current is typical. Variation in the current source will create some variation in the voltage drop across a diode junction.

A.2 Technical datasheet Agilent 34970A Datalogger

34970A/34972A accuracy specifications ±(% of reading + % of range)[1]

Includes measurement error, switching error, and transducer conversion error

	Range [3]	Frequency, etc.	24 hour [2] 23 ±1°C	90 Day 23 ±5°C	1 Year 23 ±5°C	Temperature coefficient 0 – 18°C, 28 - 55°C
DC voltage						
	100.0000 mV		0.0030 + 0.0035	0.0040 + 0.0040	0.0050 + 0.0040	0.0005 + 0.0005
	1.000000 V		0.0020 + 0.0006	0.0030 + 0.0007	0.0040 + 0.0007	0.0005 + 0.0001
	10.00000 V		0.0015 + 0.0004	0.0020 + 0.0005	0.0035 + 0.0005	0.0005 + 0.0001
	100.0000 V		0.0020 + 0.0006	0.0035 + 0.0006	0.0045 + 0.0006	0.0005 + 0.0001
	300.000 V		0.0020 + 0.0020	0.0035 + 0.0030	0.0045 + 0.0030	0.0005 + 0.0003
True RMS AC voltage [4]						
	All ranges from 100.0000 mV to 100.0000 V	3 Hz–5 Hz	1.00 + 0.03	1.00 + 0.04	1.00 + 0.04	0.100 + 0.004
		5 Hz–10 Hz	0.35 + 0.03	0.35 + 0.04	0.35 + 0.04	0.035 + 0.004
		10 Hz–20 kHz	0.04 + 0.03	0.05 + 0.04	0.06 + 0.04	0.005 + 0.004
		20 kHz–50 kHz	0.10 + 0.05	0.11 + 0.05	0.12 + 0.05	0.011 + 0.005
		50 kHz–100 kHz	0.55 + 0.08	0.60 + 0.08	0.60 + 0.08	0.060 + 0.008
		100 kHz–300 kHz [5]	4.00 + 0.50	4.00 + 0.50	4.00 + 0.50	0.20 + 0.02
	300.0000 V	3 Hz–5 Hz	1.00 + 0.05	1.00 + 0.08	1.00 + 0.08	0.100 + 0.008
		5 Hz–10 Hz	0.35 + 0.05	0.35 + 0.08	0.35 + 0.08	0.035 + 0.008
		10 Hz–20 kHz	0.04 + 0.05	0.05 + 0.08	0.06 + 0.08	0.005 + 0.008
		20 kHz–50 kHz	0.10 + 0.10	0.11 + 0.12	0.12 + 0.12	0.011 + 0.012
		50 kHz–100 kHz	0.55 + 0.20	0.60 + 0.20	0.60 + 0.20	0.060 + 0.020
		100 kHz–300 kHz [5]	4.00 + 1.25	4.00 + 1.25	4.00 + 1.25	0.20 + 0.05
Resistance [6]						
	100.0000 Ω	1 mA current source	0.0030 + 0.0035	0.008 + 0.004	0.010 + 0.004	0.0006 + 0.0005
	1.000000 kΩ	1 mA	0.0020 + 0.0006	0.008 + 0.001	0.010 + 0.001	0.0006 + 0.0001
	10.00000 kΩ	100 µA	0.0020 + 0.0005	0.008 + 0.001	0.010 + 0.001	0.0006 + 0.0001
	100.0000 kΩ	10 µA	0.0020 + 0.0005	0.008 + 0.001	0.010 + 0.001	0.0006 + 0.0001
	1.000000 MΩ	5.0 µA	0.002 + 0.001	0.008 + 0.001	0.010 + 0.001	0.0010 + 0.0002
	10.00000 MΩ	500 nA	0.015 + 0.001	0.020 + 0.001	0.040 + 0.001	0.0030 + 0.0004
	100.0000 MΩ	500 nA ‖ 10 MΩ	0.300 + 0.010	0.800 + 0.010	0.800 + 0.010	0.1500 + 0.0002
Frequency and period [7]						
	100 mV to 300V	3 Hz–5 Hz	0.10	0.10	0.10	0.005
		5 Hz–10 Hz	0.05	0.05	0.05	0.005
		10 Hz–40 Hz	0.03	0.03	0.03	0.001
		40 Hz–300 kHz	0.006	0.01	0.01	0.001
DC current (34901A only)						
	10.00000 mA	<0.1 V burden	0.005 + 0.010	0.030 + 0.020	0.050 + 0.020	0.002+ 0.0020
	100.0000 mA	<0.6 V	0.010 + 0.004	0.030 + 0.005	0.050 + 0.005	0.002 + 0.0005
	1.000000 A	<2 V	0.050 + 0.006	0.080 + 0.010	0.100 + 0.010	0.005 + 0.0010
True RMS AC current (34901A only)						
	10.00000 mA and [4]	3 Hz–5 Hz	1.00 + 0.04	1.00 + 0.04	1.00 + 0.04	0.100 + 0.006
		5 Hz–10 Hz	0.30 + 0.04	0.30 + 0.04	0.30 + 0.04	0.035 + 0.006
	1.000000 A	10 Hz–5 kHz	0.10 + 0.04	0.10 + 0.04	0.10 + 0.04	0.015 + 0.006
	100.0000 mA [8]	3 Hz–5 Hz	1.00 + 0.5	1.00 + 0.5	1.00 + 0.5	0.100 + 0.06
		5 Hz–10 Hz	0.30 + 0.5	0.30 + 0.5	0.30 + 0.5	0.035 + 0.06
		10 Hz–5 kHz	0.10 + 0.5	0.10 + 0.5	0.10 + 0.5	0.015 + 0.06

Temperature	Type	1-year accuracy [9]		Extended range 1-year accuracy [9]		Temp coefficient/°C
Thermocouple [10]	B	1100 to 1820°C	1.2°C	400 to 1100°C	1.8°C	
	E	–150 to 1000°C	1.0°C	–200 to -150°C	1.5°C	
	J	–150 to 1200°C	1.0°C	–210 to -150°C	1.2°C	
	K	–100 to 1200°C	1.0°C	–200 to -100°C	1.5°C	0.03°C
	N	–100 to 1300°C	1.0°C	–200 to -100°C	1.5°C	
	R	300 to 1760°C	1.2°C	–50 to 300°C	1.8°C	
	S	400 to 1760°C	1.2°C	–50 to 400°C	1.8°C	
	T	–100 to 400°C	1.0°C	–200 to -100°C	1.5°C	
RTD	R0 from 49 Ω to 2.1 kΩ	–200 to 600°C	0.06°C			0.003°C
Thermistor	2.2 k, 5 k, 10 k	–80 to 150°C	0.08°C			0.002°C

[1] Specifications are for 1 hr warm-up and 6½ digits, Slow ac filter
[2] Relative to calibration standards
[3] 20% over range on all ranges except 300 Vdc and ac ranges and 1 Adc and ac current ranges
[4] For sinewave input > 5% of range. For inputs from 1% to 5% of range and < 50 kHz, add 0.1% of range additional error
[5] Typically 30% of reading error at 1 MHz, limited to 1 x 108 V Hz

[6] Specifications are for 4- wire ohms function or 2-wire ohms using scaling to remove the offset. Without scaling, add 4 Ω additional error in 2-wire Ohms function
[7] Input > 100 mV. For 10 mV to 100 mV inputs multiply % of reading error x 10
[8] Specified only for inputs >10 mA
[9] For total measurement accuracy, add temperature probe error
[10] Thermocouple specifications not guaranteed when 34907A module is present. For < 1°C accuracy, a precision external reference is required.

Academic year 2020/2021

Measurement characteristics[7]

DC voltage

Measurement Method	Continuously Integrating Multi-slope III A-D converter
A/D linearity	0.0002% of reading + 0.0001 % of range
Input resistance	
100 mV, 1 V, 10 V ranges	Selectable 10 MΩ or > 10,000 MΩ
100 V, 300 V ranges	10 MΩ ±1%
Input bias current	< 30 pA at 25°C
Input protection	300 V all ranges

True RMS AC voltage

Measurement method	AC coupled True RMS — measures the AC component of the input with up to 300 Vdc of bias on any range
Crest factor	Maximum of 5:1 at Full Scale
Additional crest factor errors (non-sinewave)	
Crest Factor 1-2	0.05 % of reading
Crest Factor 2-3	0.15 % of reading
Crest Factor 3-4	0.30 % of reading
Crest Factor 4-5	0.40 % of reading
Input impedance	1 MΩ ±2% in parallel with 150 pF
Input protection	300 Vrms all ranges

Resistance

Measurement method	Selectable 4-wire or 2-wire Ohms Current source referenced to LO input
Offset compensation	Selectable on 100 Ω, 1 kΩ, 10 kΩ ranges
Maximum lead resistance	10% of range per lead for 100 Ω and 1 kΩ ranges. 1 kΩ on all other ranges
Input protection	300 V on all ranges

Frequency and period

Measurement method	Reciprocal counting technique
Voltage ranges	Same as AC Voltage function
Gate time	1s, 100 ms, or 10 ms
Measurement timeout	Selectable 3 Hz, 20 Hz, 200 Hz LF limit

DC current

Shunt resistance	5Ω for 10 mA, 100 mA; 0.1 Ω for 1 A
Input protection	1 A 250 V fuse on 34901A module

True RMS AC current

Measurement method	Direct coupled to the fuse and shunt. AC coupled True RMS measurement (measures the ac component only)
Shunt resistance	5 Ω for 10 mA; 0.1 Ω for 100 mA, 1 A
Input protection	1 A 250 V fuse on 34901A module

Thermocouple

Conversion	ITS-90 software compensation
Reference junction type	Internal, Fixed, or External
Open thermocouple check	Selectable per channel. Open > 5 kΩ

Thermistor 44004, 44007, 44006 series

RTD α = 0.00385 (DIN) and α = 0.00391

Measurement noise rejection 60 (50) Hz [1]

dc CMRR	140 dB
ac CMRR	70 dB
Integration time	**Normal mode rejection[2]**
200 plc/3.33s (4s)	110 dB [3]
100 plc/1.67s (2s)	105 dB [3]
20 plc/333 ms (400 ms)	100 dB [3]
10 plc/167 ms (200 ms)	95 dB [3]
2 plc/33.3 ms (40 ms)	90 dB
1 plc/16.7 ms (20 ms)	60 dB
< 1 plc	0 dB

Operating characteristics [4]

Single channel measurement rates [5]

Function	Resolution [8]	34970A/34972A readings/sec
dcV, 2-wire resistance	6½ digits (10 plc)	6 (5)
	5½ digits (1 plc)	54 (47)
	4½ digits (0.02 plc)	500
Thermocouple	0.1 °C (10 plc)	6 (5)
	0.1 °C (1 plc)	52 (47)
	(0.02 plc)	280
RTD, thermistor	0.01 °C (10 plc)	6 (5)
	0.1 °C (1 plc)	49 (47)
	1 °C (0.02 plc)	200
acV	6½ Slow (3 Hz)	0.14
	6½ Med (20 Hz)	1
	6½ Fast (200 Hz)	8
	6½ [6]	100
Frequency, period	6½ digits (1 s gate)	1
	5½ digits (100 ms)	9
	4½ digits (10 ms)	70

[1] For 1 KΩ unbalance in LO lead
[2] For power line frequency ±0.1%
[3] For power line frequency ±1% use 80 dB or ±3% use 60 dB
[4] Reading speeds for 60 Hz and (50 Hz) operation
[5] For fixed function and range, readings to memory, scaling and alarms off, AZERO OFF, USB datalogging OFF
[6] Maximum limit with de fault settling delays defeated
[7] Isolation voltage (ch-ch, ch-earth) 300 Vdc, ac rms
[8] 6½ digits = 22 bits, 5½ digits = 18 bits, 4½ digits = 15 bits

86

A.3 Technical datasheet Agilent 34901A 20-Channel General Purpose Multiplexer

Multiplexer selection guide

Choose between the broad functionality of the 34901A, the high speed scanning of the 34902A, or the single-ended density of the 34908A. These three modules are the only way to connect to the 34970A/34972A internal DMM. They can be used to scan with external instruments as well.

All multiplexer modules employ break-before-make scanning, ensuring only one closed channel (or channel pair) at a time. Multiple channel closures are allowed on the 34901A and 34902A modules when not configured for scanning.

The 34908A does not allow multiple channel closures at any time.

34901A

	34901A	34902A	34908A
Number of channels	20 + 2	16	40
Max scan speed	60 ch/s	250 ch/s	60 ch/s
Number of contacts	2 or 4	2 or 4	1
Temperature			
Thermocouple	●	●	●
2-wire RTD	●	●	●
4-wire RTD	●	●	
Thermistor	●	●	●
dc Volts	●	●	●
ac Volts	●	●	●
2-wire Ohms	●	●	●
4-wire Ohms	●	●	
Frequency	●	●	●
Period	●	●	●
dc current	●		
ac current	●		

20-Channel General Purpose Multiplexer

– 60 ch/s scanning
– Two- and four-wire scanning
– Built-in thermocouple reference junction
– 300 V switching

The Keysight 34901A is the most versatile multiplexer for general purpose scanning. It combines dense, multifunction switching with 60-channel/second scan rates to address a broad spectrum of data acquisition applications.

Two- and four-wire channels can be mixed on the same module. Two additional fused inputs (22 channels total) route up to 1 A of current to the internal DMM, allowing ac and dc current measurements without the need for external shunt resistors.

87

A.5 Technical datasheet Kipp and Zonnen CMP11 Pyranometer

Technical Specifications

|	CMP10 | CMP11	SMP10 | SMP11
Classification to ISO 9060:2018	Spectrally Flat Class A	Spectrally Flat Class A
Sensitivity	7 to 14 µV/W/m²	-
Impedance	10 to 100 Ω	-
Expected output range (0 to 1500 W/m²)	0 to 20 mV	-
Maximum operational irradiance	4000 W/m²	-
Analog output • V-version	-	0 to 1 V
Analog output range*	-	-200 to 2000 W/m²
Analog output • A-version	-	4 to 20 mA
Analog output range*	-	0 to 1600 W/m²
Serial output	-	RS-485 Modbus®
Serial output range	-	-400 to 4000 W/m²
Response time (63 %)	< 1.7 s	< 0.7 s
Response time (95 %)	< 5 s	< 2 s
Spectral range (20 % points)	270 to 3000 nm	270 to 3000 nm
Spectral range (50 % points)	285 to 2800 nm	285 to 2800 nm
Zero offsets (unventilated) (a) thermal radiation (at 200 W/m²) (b) temperature change (5 K/h)	< 7 W/m² < 2 W/m²	< 7 W/m² < 2 W/m²
Non-stability (change/year)	< 0.5 %	< 0.5 %
Non-linearity (100 to 1000 W/m²)	< 0.2 %	< 0.2 %
Directional response (up to 80 ° with 1000 W/m² beam)	< 10 W/m²	< 10 W/m²
Spectral selectivity (350 to 1500 nm)	< 3 %	< 3 %
Tilt response (0 ° to 90 ° at 1000 W/m²)	< 0.2 %	< 0.2 %
Temperature response	< 1 % (-10 °C to +40 °C)	< 1 % (-20°C to +50 °C) < 2 % (-40 °C to +70 °C)
Field of view	180 °	180 °
Accuracy of bubble level	< 0.1 °	< 0.1 °
Power consumption (at 12 VDC)	-	V-version: 55 mW A-version: 100 mW
Supply voltage	-	5 to 30 VDC
Software, Windows™	-	SmartExplorer Software, for configuration, test and data logging
Detector type	Thermopile	Thermopile
Operating and storage temperature range	-40 °C to +80 °C	-40 °C to +80 °C
Humidity range	0 to 100 %	0 to 100 %
MTBF (Mean Time Between Failures)	> 10 years	> 10 years **
Ingress Protection (IP) rating	67	67
Recommended applications	Meteorological networks, PV panel and thermal collector testing, materials testing	High performance for PV panel and thermal collector testing, solar energy research, solar prospecting, materials testing, advanced meteorology and climate networks

Note: The performance specifications quoted are worst-case and/or maximum values.
* adjustable with SmartExplorer Software | ** extrapolated after introduction in January 2012

Dimensions

CMP10 | SMP10   Ø 50 mm   68 mm   Ø 150 mm

CMP11 | SMP11   Ø 50 mm   68 mm   Ø 150 mm
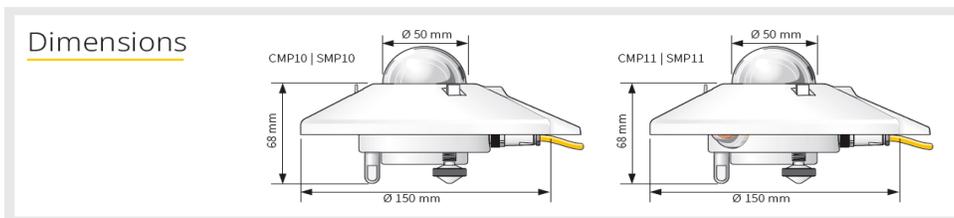
A.6 Technical datasheet Kipp and Zonnen CHP1 Pyrheliometer

74 mm · 322 mm · Ø38 mm · 76 mm

Specifications	CHP 1	SHP1
ISO 9060:1990 CLASSIFICATION	First Class	First Class
Response time (63 %)	< 1.7 s	< 0.7 s
Response time (95 %)	< 5 s	< 2 s
Zero offsets due to temperature change (5 K/hr)	< 1 W/m²	< 1 W/m²
Non-stability (change/year)	< 0.5 %	< 0.5 %
Non-linearity (0 to 1000 W/m²)	< 0.2 %	< 0.2 %
Temperature dependence of sensitivity	< 0.5 % (-20 °C to +50 °C)	< 0.5 % (-30 °C to +60 °C)
Sensitivity	7 to 14 µV/W/m²	NA
Other specifications		
Analogue output	10 to 20 mV for 1400 W/m²	-V version: 0 to 1 V -A version: 4 to 20 mA
Analogue output range	0 to 4000 W/m²	-V version: -200 to 2000 W/m² [1] -A version: 0 to 1600 W/m²
Digital output	NA	2-wire RS-485, Modbus® protocol
Operating temperature	-40 °C to +80 °C	-40 °C to +80 °C
Full viewing angle	5° ±0.2°	5° ±0.2°
Maximum irradiance	4000 W/m²	4000 W/m²
Humidity	0 to 100 % RH	0 to 100 % RH
Spectral range (50 % points)	200 to 4000 nm	200 to 4000 nm
Required sun tracker accuracy	< 0.5° from ideal	< 0.5° from ideal
Weight (excluding cable)	0.9 kg	0.9 kg
Slope angle	1° ±0.2°	1° ±0.2°
Temperature sensor	Both Pt-100 and 10k thermistor as standard [2]	Internal [3]
Supply voltage	NA	5 to 30 VDC
Power consumption (at 12 VDC)	NA	-V version: 55 mW -A version: 100 mW
Expected daily uncertainty	< 1 %	< 1 %
Documentation	Calibration certificate traceable to WRR, multi-language instruction sheet, manual on CD-ROM	
Recommended applications	High performance direct radiation monitoring for meteorological stations or concentrated solar energy applications	

[1] The analogue output range of SHP1 can be rescaled by the user to a maximum of -200 to 4000 W/m²

[2] Supplied with individual temperature dependence test data

[3] Output data individually temperature corrected for each SHP1 over -40 °C to +70 °C

Pyheliometers have a standard cable length of 10 m. Optional cable lengths 25 m and 50 m

Note: The performance specifications quoted are worst-case and/or maximum values

KIPP & ZONEN
SINCE 1830

Go to www.kippzonen.com for your local distributor

89

A.7 Technical datasheet Eko MS-700 Spectroradiometer

EKO MS-700 Specifications *(Typical)*		
Sensor head	**MS-700**	**MS-700 DNI**
Wavelength range	350 to 1050 nm	
Wavelength interval	3.3 nm	
Spectral resolution FWHM	10 nm	
Wavelength accuracy	<0.3 nm	
Exposure time	10 ms to 5 s	
Temp. dependency (−20° to 50°C)	$< \pm 1\,\%$	
Temperature control	$25 \pm 5^{\circ}C$	
Cosine response (0° to 80°)	<7%	–
Aperture	180°	5°
Slope angle	–	1°
Stray light	0.15%	
Window material	Optical glass	Quartz glass
Communication	RS-422 (Between head and power supply)	
Cable length	10 m (Optional max. 30 m)	
Power requirements	12 Vdc, 50 VA (power supply)	
Operating temperature range (°C)	−20 to +50	
Dimensions (sensor)	200(φ)×175(H) mm (With sun screen: 240(φ)×175(H) mm)	200(φ)×300(H) mm
Weight (sensor)	4 kg	4.5 kg
Power supply		
AC supply voltage	AC100-240V, 50/60 Hz, 50 VA	
DC supply voltage	DC 12 V	
Operating environment	Temperature: 0° to 40°C, Relative Humidity: 0 to 90%, non-condensing	
Dimensions	200 (W) x 140 (D) x 80 (H) mm	
Weight	1 kg	

A.8 Technical datasheet Tri-band Spectro- Heliometer IES-UPM ICU-3J24

POLITÉCNICA IES-UPM

Tri-band Spectro-heliometer ICU-3J24

This SPECTROHELIOMETER measures the effective irradiance in the spectral zones corresponding to the top, middle, and bottom subcells of a lattice-matched GaInP / GaAs / Ge triple-junction solar cell.

The SPECTROHELIOMETER can be used to monitor the spectral content of solar radiation in a way that is meaningful for predicting performance of such cells, or of concentrator systems that use them.

CALIBRATION

The sensor has been calibrated outdoors by comparison with reference sensor under clear sky conditions simultaneously to the reference sensor. Calibration is traceable to balloon flight standards.

TRACKING

With a field of view limited to 5.7°, TRI-BAND SPECTROHELIOMETER measures only the direct beam solar irradiance, thanks to the collimation tube and the specific apertures. It therefore must be mounted on a Solar Tracker and pointed at the sun at all time. The TRI-BAND SPECTROHELIOMETER is designed to be easily installed in any tracker configuration, either mounted flat to a plane perpendicular to the solar vector, or mounted atop an existing normal insolation pyrheliometer.

SUGGESTED USE

- Measure of spectral radiation effects
- Prediction of current mismatch between subcells of a lattice-matched GaInP / GaAs / Ge triple-junction solar cell.
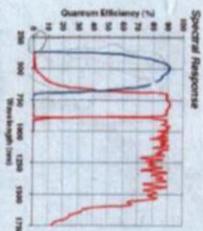
SPECIFICATIONS

	Top	DLE	Bottom
SPECTRAL RANGE	375 - 700 nm	nm	900 - 1700 nm
TEMPERATURE DEPENDENCE OF SENSITIVITY	< 0.1%		< 0.05%
LINEARITY	±2%		
FULL OPENING VIEW ANGLE	±2.8° (collimation t)		
SLOPE ANGLE	±2.3°		
RESPONSE TIME	< 1 μs		
OUTPUT IMPEDANCE	47 Ω		27 Ω
OUTPUT SIGNAL (0 - 1300 W/m²)	6-100 mV		
OPERATION TEMPERATURE	-40° - 80°		
WINDOW MATERIAL	Fused silica		
BODY CONSTRUCTION	Aluminum		
DESICCANT	Silica gel (orange)		
WEIGHT (EXCLUDING CABLE)	1.5 kg		
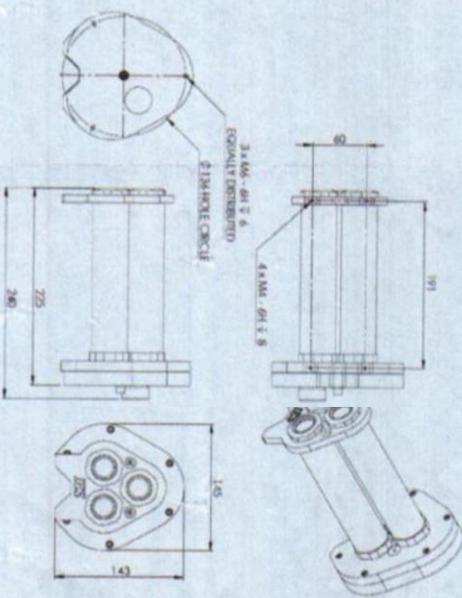
POLITÉCNICA

http://www.ies.upm.es/

INSTITUTO DE ENERGIA SOLAR
E.T.S.I. TERICACIÓN -
CIUDAD UNIVERSITARIA
28040 - SPAIN

Telf. (+34) 910 / 91 543 11 98
Fax: (+34) 63 41
info@ies.es

A.9 Technical datasheet Young 05305VM anemometer

MODEL 05305V
WIND MONITOR-AQ
with VOLTAGE OUTPUTS

WIND SPEED SPECIFICATION SUMMARY

Range	0 to 40 m/s (90 mph), gust survival 100 m/s (220 mph)
Sensor	20 cm diameter 4-blade helicoid carbon fiber thermoplastic propeller, 30.7 cm air passage per revolution
Distance Constant	2.1 m (6.9 ft.) for 63% recovery
Threshold Sensitivity	0.4 m/s (0.9 mph)
Transducer	Centrally mounted stationary coil, 2K Ohm nominal DC resistance
Output Signal	0 to 1.00 VDC over specified range

Model No. Suffix	Range
M	0 to 50 M/S
P	0 to 100 MPH
N	0 to 100 KNOTS
K	0 to 200 KILOMETERS/HOUR

WIND DIRECTION (AZIMUTH) SPECIFICATION SUMMARY

Range	360° mechanical, 355° electrical (5° open)
Sensor	Balanced vane, 48.3 cm (19 in) turning radius.
Damping Ratio	0.45
Delay Distance	1.2 m (3.9 ft) for 50% recovery
Threshold Sensitivity	0.5 m/s (1.0 mph) at 10° displacement
Damped Natural Wavelength	4.9 m (16.1 ft)
Undamped Natural Wavelength	4.4 m (14.4 ft)
Transducer	Precision conductive plastic potentiometer, 10K ohm resistance (±20%), 0.25% linearity, life expectancy 50 million revolutions, rated 1 watt at 40°C, 0 watts AT 125°C
Output Signal	0 to 1.00 VDC for 0 to 360°

GENERAL

Power Requirement: 8 - 24 VDC (5mA @ 12 VDC)
Operating Temperature: -50 to 50°C (-58 to 122°F)

INTRODUCTION

The Wind Monitor measures horizontal wind speed and direction. Developed for air quality applications, it is accurate, sensitive, and corrosion resistant. The main housing, nose cone, propeller, and other internal parts are injection molded U.V. stabilized plastic. The tail section is lightweight expanded polystyrene. Both the propeller and vertical shafts use stainless steel precision grade ball bearings. Bearings have shields to help exclude contamination and moisture.

Propeller rotation produces an AC sine wave signal with frequency proportional to wind speed. Internal circuitry converts the raw signal to a linear voltage output.

Vane position is sensed by a 10K ohm precision conductive plastic potentiometer. This signal is also converted to voltage output.

The instrument mounts directly on standard one inch pipe, outside diameter 34 mm (1.34"). An orientation ring is provided so the instrument can be removed for maintenance and re-installed without loss of wind direction reference. Both the sensor and the orientation ring are secured to the mounting pipe by stainless steel band clamps. Electrical connections are made in a junction box at the base.

INITIAL CHECKOUT

When the Wind Monitor is unpacked it should be checked carefully for any signs of shipping damage.

Remove the plastic nut on the propeller shaft. Install the propeller on the shaft with the serial number of the propeller facing forward (into the wind). The instrument is aligned, balanced and fully calibrated before shipment; however, it should be checked both mechanically and electrically before installation. The vane and propeller should easily rotate 360° without friction. Check vane balance by holding the instrument base so the vane surface is horizontal. It should have near neutral torque without any particular tendency to rotate. A slight imbalance will not degrade performance.

INSTALLATION

Proper placement of the instrument is very important. Eddies from trees, buildings, or other structures can greatly influence wind speed and wind direction observations. To get meaningful data for most applications, locate the instrument well above or upwind from obstructions. As a general rule, the air flow around a structure is disturbed to twice the height of the structure upwind, six times the height downwind, and up to twice the height of the structure above ground. For some applications it may not be practical or necessary to meet these requirements.

FAILURE TO PROPERLY GROUND THE WIND MONITOR MAY RESULT IN ERRONEOUS SIGNALS OR TRANSDUCER DAMAGE.

Grounding the Wind Monitor is vitally important. Without proper grounding, static electrical charge can build up during certain atmospheric conditions and discharge through the transducers. This discharge may cause erroneous signals or transducer failure.

92

A.10 Technical datasheet Young 41382VC Relative Humidity and Temperature Probe

MODEL 41382VC
RELATIVE HUMIDITY / TEMPERATURE PROBE
with VOLTAGE OUTPUT

**INSTRUCTION SHEET 41382VC-90**
REV E102613

INTRODUCTION

The Model 41382VC Relative Humidity/Temperature Probe combines high accuracy humidity and temperature sensors in a single probe. The output signal is 0-1 V (standard) or 0-5 V (user selected option) for both relative humidity and temperature. RH range is 0-100%. Temperature range is -50 to +50°C.

INSTALLATION

Install the probe in a naturally ventilated or fan aspirated radiation shield. Mount probe and shield in a location with good air circulation clear of large thermal masses (buildings, pavement, solar panels, etc.), exhaust vents, electrical machinery and motors, water fountains and sprinklers.

Set 0-1 V or 0-5 V output with jumpers as shown in diagram. These jumpers are located below the terminals in the junction box.

VOLTAGE OUTPUT SELECTION JUMPERS

RH TEMP 5 1 0-1V POSITION (STANDARD)

RH TEMP 5 1 0-5V POSITION
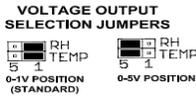
MAINTENANCE

The probe provides years of service with minimal maintenance. Humidity calibration, which may drift slightly with time, can be checked or restored at the factory.

Periodically clean the humidity sensor filter when used in areas of high dust or contamination (smokestacks, seawater, etc.) Soak in clean water or use a mild soap solution. DO NOT USE SOLVENTS.

CE COMPLIANCE

This product complies with the European CE directive on EMC compatibility. Shielded cable must be used.

WARRANTY

This product is warranted to be free of defects in materials and construction for a period of 12 months from date of initial purchase. Liability is limited to repair or replacement of defective item. A copy of the warranty policy may be obtained from R. M. Young Company.

SPECIFICATIONS

RELATIVE HUMIDITY:

Measuring range:	0-100% RH
Accuracy at 23°C:	±1%
Stability:	Better than ±1%RH per year
Response Time:	10 seconds (Without Filter)
Sensor type:	Rotronic Hygromer

TEMPERATURE:

Measuring Range:	-50 to +50°C
Accuracy at 23°C:	±0.3°C
Response Time:	10 seconds (Without Filter)
Sensor type:	Platinum RTD

Output signal:	0-1 or 0-5 VDC (jumper option)
Power Required:	8-30 VDC at 7 mA
Recommended Cable:	5 conductor shielded, Young 18446

Recommended Shields:
Young Model 43502 Aspirated Radiation Shield
Young Model 41003P Multi-Plate Radiation Shield

Declaration of Conformity

R. M. Young Company
2801 Aero Park Drive
Traverse City, MI 49686 USA

Model 41382VC RH/Temp Probe
The undersigned hereby declares on behalf of R. M. Young Company that the above-referenced product, to which this declaration relates, is in conformity with the provisions of:

Council Directive 2004/108/EC (December 15, 2004) on Electromagnetic Compatibility

David Poinsett
R&D Manager

WIRING DIAGRAM
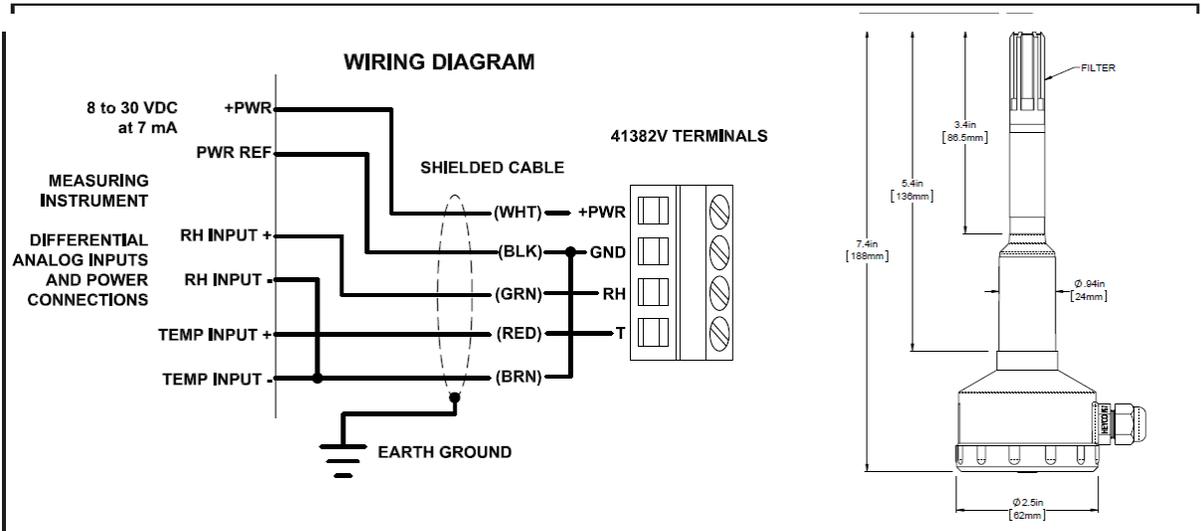
R. M. YOUNG COMPANY   2801 Aero Park Drive , Traverse City, Michigan 49686 USA
TEL (231) 946-3980   FAX (231) 946-4772

93

Annex B

B.1 Datasheet of Kyocera KD 135GH- 2PU module

THE NEW VALUE FRONTIER

KYOCERA

KD135GH-2PU

High efficiency multicrystal photovoltaic module

CUTTING-EDGE TECHNOLOGY

Exhaustive research work and continuous further development of production processes enable the integrated Kyocera high-performance solar cells with a standard size of 156 mm x 156 mm to achieve over 16 % efficiency, guaranteeing an extremely high annual yield of energy from the photovoltaic system.

To protect against the harshest weather conditions, the cells are embedded between a reinforced glass covering and EVA foil, and are sealed with a PET foil backing. The laminate is set in a sturdy aluminium frame which is easy to assemble. Our warranty covers a surface load of 2,400 N/m², but (in addition to that), the module even passed TÜV certification test IEC 61215 ed. 2 with the test condition of 5,400N/m².

The junction box on the module backside is equipped with bypass diodes that eliminate the risk of the individual solar cells overheating (hot spot effect). Many series-connected photovoltaic modules can be easily wired using pre-assembled solar cables and multi-contact plugs.

Kyocera manufactures all the components at its own production sites – without buying in semi-finished products – to ensure consistently high product quality.

EXAMPLES OF APPLICATION

· Grid-connected systems, for e.g.
  – Residential solar power systems
  – Public and industrial solar power systems
· Solar power stations

Apartment house

TUVdotCOM Service: Internet platform for tested quality and service
TUVdotCom-ID: 0000023299
IEC 61215 ed. 2, IEC 61730 and Safety Class II
Kyocera is ISO 9001 and ISO 14001 certified and registered.

TÜV   CE

KYOCERA SOLAR

We care!

SPECIFICATIONS

in mm
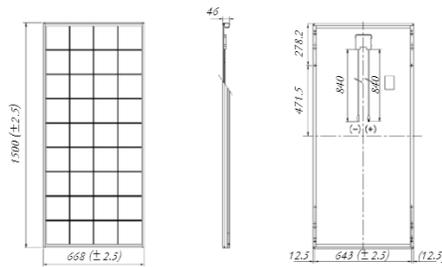
ELECTRICAL CHARACTERISTICS

Current-Voltage characteristics at various cell temperatures

Irradiance: AM 1.5, 1 kW/m²
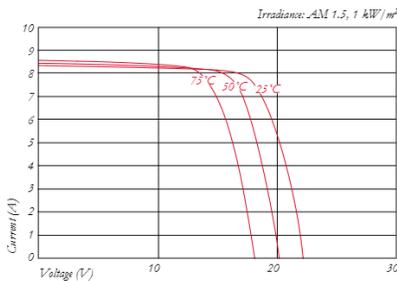
Current-Voltage characteristics at various irradiance levels

Cell temperature 25 °C
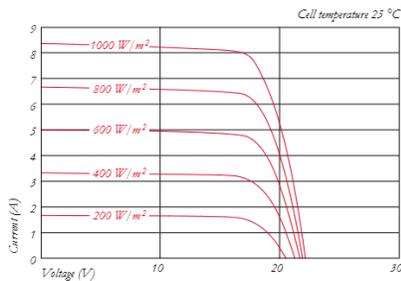
ELECTRICAL PERFORMANCE

PV Module Type		KD135CH-2PU
At 1000 W/m² (STC)*		
Maximum Power	[W]	135
Maximum System Voltage	[V]	1000
Maximum Power Voltage	[V]	17.7
Maximum Power Current	[A]	7.63
Open Circuit Voltage (V$_{OC}$)	[V]	22.1
Short Circuit Current (I$_{SC}$)	[A]	8.37
At 800 W/m² (NOCT)**		
Maximum Power	[W]	95
Maximum Power Voltage	[V]	15.6
Maximum Power Current	[A]	6.1
Open Circuit Voltage (V$_{OC}$)	[V]	19.9
Short Circuit Current (I$_{SC}$)	[A]	6.82
NOCT	[°C]	49
Power Tolerance	[%]	+5/-5
Maximum Reverse Current I$_R$	[A]	15
Series Fuse Rating	[A]	15
Temperature Coefficient of V$_{OC}$	[V/°C]	-0.80x10⁻¹
Temperature Coefficient of I$_{SC}$	[A/°C]	5.01x10⁻³
Temperature Coefficient of Max. Power	[W/°C]	-6.14x10⁻¹
Reduction of Efficiency (from 1000 W/m² to 200 W/m²)	[%]	5.8

DIMENSIONS

Length	[mm]	1500 (±2.5)
Width	[mm]	668 (±2.5)
Depth / incl. Junction Box	[mm]	46
Weight	[kg]	12.5
Cable	[mm]	(+)840 / (−)840
Connection Type		MC PV-KBT3 / MC PV-KST3
Junction Box	[mm]	100x108x15
IP Code		IP65

GENERAL INFORMATION

Performance Guarantee		10*** / 20 years****
Warranty		2 years

CELLS

Number per Module		36
Cell Technology		polycrystalline
Cell Shape (square)	[mm]	156x156
Cell Bonding		3 busbar

*   *Electrical values under standard test conditions (STC): irradiation of 1000 W/m², airmass AM 1.5 and cell temperature of 25 °C*
** *Electrical values under normal operating cell temperature (NOCT): irradiation of 800 W/m², airmass AM 1.5, wind speed of 1 m/s and ambient temperature of 20 °C*
*** *10 years on 90 % of the minimally specified power P under standard test conditions (STC)*
**** *20 years on 80 % of the minimally specified power P under standard test conditions (STC)*

Your local Kyocera dealer:

KYOCERA SOLAR

We care!

**KYOCERA Fineceramics GmbH
Solar Division**
Fritz-Mueller-Straße 27
73730 Esslingen/Germany
Tel: +49 (0)711-93 93 49 99
Fax: +49 (0)711-93 93 49 50
E-Mail: solar@kyocera.de
www.kyocerasolar.de

95